Journal of Engineering Mathematics **27**: 309–342, 1993.

On boundary-layer transition in transonic flow

R.I. BOWLES and F.T. SMITH*

Department of Mathematics, University College London, Gower Street, London WC1E 6BT, United Kingdom
(* *author for correspondence*)

Received 14 May 1992; accepted in revised form 5 November 1992

Abstract. Boundary-layer transition in transonic external flow is addressed theoretically. The transonic area is rich in different flow structures, and transition paths, and the work has wide potential application in transonic aerodynamics, including special reference to the example of flow transition over an engine nacelle. The investigation is intended partly to aid, compare with, and detect any limitations of, a quasi-parallel empirical methodology for design use in the area, especially with respect to the transonic range, and partly to develop an understanding and possible control of the nonlinear natural or by-pass properties of the compressible transition present. The mechanisms behind three major factors, (a) substantial external-flow deceleration, (b) rapid boundary-layer thickening, (c) three-dimensional nonlinear interactions, are identified; these three are involved in the specific application above and in more general configurations, depending on the disturbance background present. It is found also that some similarities exist with the phenomenon of buffeting on transonic airfoils, and the relevant physics and governing equations throughout are identified. Sensitive nonlinear effects are important in all the factors (a)–(c), especially a resonance linkage between shock buffeting and boundary-layer thickening, and nonlinearly enhanced three-dimensional growth triggered by slight three-dimensional warping for instance, peculiar to the transonic range. The latter enhanced growth is perhaps the most significant finding. The implications, in the general setting as well as for the nacelle-flow context in particular, are also presented.

1. Introduction

This paper describes research on nonlinear theory addressing boundary-layer transition in transonic flow. Little or no nonlinear theoretical study appears to have been made for transonic transition as far as we can tell; yet the area turns out to be rich in fluid-dynamic interest, on the one hand, and it has many applications in transonic flows on the other. Our study was motivated initially by concern over transition in the flow on an engine nacelle, numerous discussions of which took place between the authors and Dr Wes Lord and colleagues at Pratt and Whitney. The specific characteristics of that transitional flow in practice seem to be its transonic nature and the significant variation in pressure gradient driving the boundary layer, especially during deceleration. Other specific features of note are a slight warping of the nacelle from its axisymmetric design shape, and the possibilities of an induced shock and a rapidly increasing boundary-layer displacement, perhaps provoking separation, during the deceleration and transition. These nacelle-flow characteristics partly prompt the current research. At the start of the theoretical research a number of options had to be sifted through and considered, including different instabilities, pressure-gradient effects, mode interaction, linear and two-dimensional (2D) as opposed to nonlinear and 3D, and so on, and from among these options the main findings are described in the present paper. There is wide application however throughout the transonic regime.

Viscous-inviscid interaction almost certainly plays a key role, we feel, in many of the applications, and often in fact there may well be a close resemblance between the nacelle transition above and the phenomenon of large-scale buffeting on transonic airfoils, a

nonlinear unsteady phenomenon where, in effect, viscous-inviscid interaction takes place between the strong external disturbance (a moving shock) and strong internal responses (downstream transition and/or separation): see experiments and computations in Bogar [1], Dolling and Brusniak [2], Dolling [3] for example. The interaction when it occurs may also be regarded in some cases as a form of by-pass transition, in 2D or 3D (while in other cases it is slower transition). The major difference in the nacelle-flow context is a matter of the smaller length scales involved. So a nonlinear linkage between the unsteady flows inside and outside the compressible boundary layer seems essential in such cases, and that provides part of the present focus. The linkage, and the unsteadiness, point directly to an examination of unsteady interactive boundary layers (IBL) and Tollmien–Schlichting (TS)-like waves but with emphasis on nonlinearity and transonic flow. The idea in such cases is that the external disturbance, e.g. due to an oscillating shock or flow deceleration, can set up an adverse pressure gradient sufficient to trigger boundary-layer transition, which in turn then alters the external flow and reinforces the shock movement, and hence the whole 2D or 3D interaction.

Given that setting, an aim here is to account for the significant effects of: (a) substantial external-flow deceleration, (b) rapid boundary-layer thickening, (c) 3D nonlinear interactions (e.g. stemming from warping), in transonic boundary-layer transition. The 2D nonlinear theory discussed in Section 2 below provides a useful starting point, with Sections 3 and 4 then moving on from there, to tackle the particular characteristics (a)–(c) above. The above features may appear to be rather particular of course, but the present work also addresses transonic transition more generally as we see below.

We concentrate throughout on transition properties that are specific to the transonic range. It is true that there is no completely satisfactory transition theory as yet for flow at any free-stream Mach number M_∞, despite a large amount of literature (e.g. Van Driest and Blumer [4], Dunham [5], Arnal [6], Morkovin [7], Smith [8], Roberts [9], Abu-Ghannam and Shaw [10], Narasimha [11], Gostelow and Blunden [12], Smith and Gamberoni [13], Van Ingen [14], Cebeci and Egan [15], Cebeci [16]) on the theoretical and experimental aspects and empirical transition criteria at various flow speeds. Nevertheless, the nearest so far to such a transition theory seems to be that being developed for high Reynolds numbers Re described in Smith [17–19, 20, 21, 8], et al. [22–28], Bowles [29], for examples, mainly for the incompressible regime but more recently for compressible boundary layers (Smith [21], Smith and Walton [28], Bowles [29], Hall and Smith [30], Brown et al. [31]), and here we adopt that general theoretical approach. The approach tends to distinguish between gradual transition and by-pass transition, dependent upon the input frequencies, amplitudes and wavenumbers. The former route typically has linear 2D TS disturbance growth first, say on a flat plate, then 2D nonlinear growth and 3D secondary instability, closely followed downstream by strong 3D nonlinear focusing, amplification and break-up, possibly leading then to turbulence. The successive 2D and 3D stages involved, including resonant-triad interactions, 3D focusing and induced Euler-scale interactions, are described in the references above, as is the by-pass transition route which essentially activates the later high-amplitude stages directly. The approach has been shown (Smith and Stewart [25], Smith [21], Smith, Papageorgiou and Elliott [32]) to agree quantitatively and/or qualitatively with experiments and direct Navier–Stokes simulations, although the latter are confined still to relatively low Re, and it suggests the application of IBL methods for transition prediction. In the present context, a number of new features unique to the transonic range are identified.

The 2D transonic range addressed in Section 2 is found to produce broadly the same linear

and nonlinear properties as arise in the pure subsonic or supersonic regimes, with some notable exceptions, e.g. at higher amplitudes. The alternative 2D nonlinear range in Section 3, however, shows two substantially different aspects arising, namely external shock effects and internal separation effects, corresponding to (a), (b) above. The nonlinear linkage between (a), (b) provides a by-pass mechanism (as in buffeting or shock flutter) which is potentially powerful locally and could readily induce transition. Likewise, the 3D influence (Section 4) corresponding to (c) above turns out to be very important, in particular yielding substantial differences between linear and nonlinear behaviour and between 2D- and 3D-based predictions, in the transonic range. Thus new forms of three-wave resonance, of strong 3D nonlinear growth with focusing, and of vortex-wave interactions, are found throughout the transonic regime, along with a distinct effect produced by slight 3D warping of an otherwise 2D input disturbance upstream. This last is perhaps the finding of most interest and may be of significance for the nacelle configuration outlined at the start of this section as well as in other transonic-flow applications. Both slight warping, i.e. the low-spanwise-wavenumber content of the input, and enhanced 3D input, at much higher spanwise wavenumbers, provoke spatial focusing and amplification fast nonlinearly, in contrast with the spanwise wavenumbers in-between and with 2D theory. These and other 3D aspects (among which we should mention especially the so-called major mode) are described in Section 4, while Section 5 provides further discussion of the overall features including comments on alternative theory, e.g. e^N methods, on alternative transition routes for the transonic boundary layer (see [17]), and on implications for the nacelle-flow context in particular.

Notation. Nondimensional velocity components (u, v, w) and corresponding cartesian coordinates (x, y, z) are used such that the local planar external flow speed and the characteristic length scale, e.g. airfoil chord, are both 1, with the pressure p, density ρ, temperature T, viscosity μ and time t being nondimensionalized similarly. The corresponding Reynolds number Re is large, the Mach number M_∞ is usually taken to be near unity, and the Chapman viscosity law is assumed without loss of generality. Locally the body surface coincides with $y = 0$, and x, z are the streamwise and spanwise coordinate in turn, while the oncoming boundary-layer thickness at the station $(x_0, 0, z_0)$ in question is of the order $\mathrm{Re}^{-1/2}$.

2. Transonic unsteady interaction

In this section, the linear and nonlinear unsteady-flow features of a first transonic stage, regime I defined by (2.2) below, are considered with regard to transition. Several distinct transonic properties are found, and the theory also provides a lead-in to the transonic transition properties investigated in Sections 3 and 4 concerning a second transonic regime and 3D features. The following sub-sections deal with the transonic stage I, the nonlinear high-frequency response, higher-amplitude phenomena, and the Euler stage with related comments, in turn (see also Fig. 1).

2.1. Transonic stage I

We start by comparing the typical wave speed and the speed of sound in the free stream. In pure subsonic or supersonic flow, information travels much faster in the outer free stream,

upstream or downstream, than the rate associated with the relatively slow TS waves, and so in TS interactions the outer response is then quasi-steady. In a transonic stream, by contrast, the outer rate of travel is slow, and it turns out that a significant new regime comes into operation when the two rates, that of free-stream propagation and that typical of TS waves becomes comparable.

The new unsteady transonic regime is found, after some working, to be given by the following triple-deck scales around a typical station x_0, z_0:

$$[x - x_0, z - z_0, t] = [\mathrm{Re}^{-3/9} b_1 X, \mathrm{Re}^{-5/18} b_4 Z, \mathrm{Re}^{-2/9} b_2 T], \tag{2.1a}$$

$$y = \mathrm{Re}^{-11/18} b_3 Y \text{ (lower deck)}, \qquad y = \mathrm{Re}^{-5/18} b_4 \bar{y} \text{ (upper deck)}, \tag{2.1b}$$

$$[u, v, w, p - p_\infty] = [\mathrm{Re}^{-1/9} b_5 U, \mathrm{Re}^{-7/18} b_6 V, \mathrm{Re}^{-1/18} b_5 b_4 b_1^{-1} W, \mathrm{Re}^{-2/9} b_7 P] \tag{2.1c}$$

at large Re, where (2.1c) holds for the lower deck, nearest the wall, the main deck corresponds to the $O(\mathrm{Re}^{-1/2})$ y-scaling of the oncoming boundary layer, and the upper deck

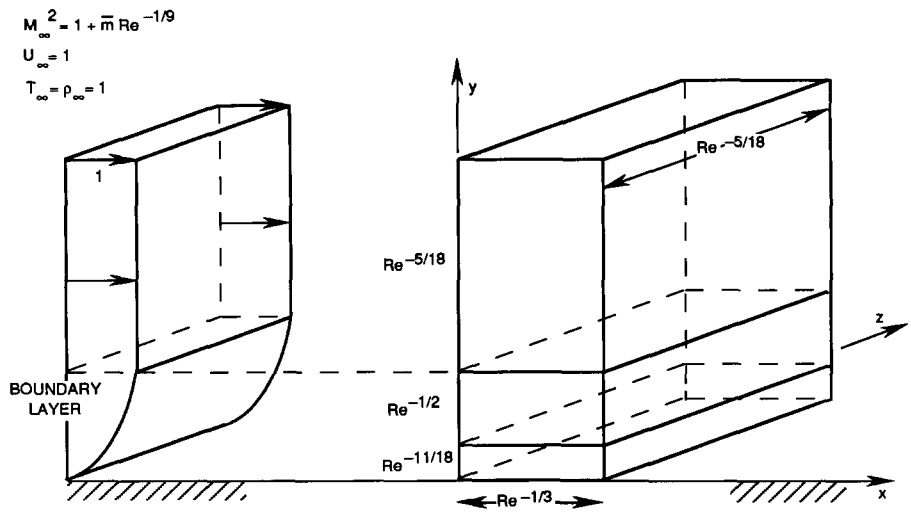

Fig. 1(a). Disturbance structure.

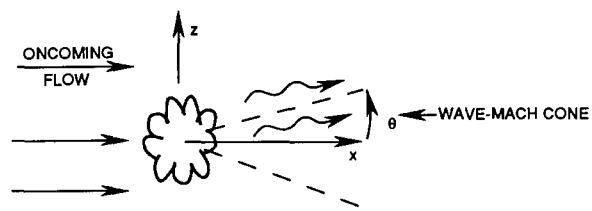

Fig. 1(b). Disturbances directed inside wavecone.

Fig. 1. (a) Nonlinear disturbance structure for regime I, where $\mathrm{M}_\infty^2 - 1 = O(\mathrm{Re}^{-1/9})$. A 2D oncoming flow is subjected to a 3D disturbance of small angle θ to the oncoming flow, inside the wave-Mach cone with $\tan\theta \sim (\mathrm{M}_\infty^2 - 1)^{1/2} \sim \mathrm{Re}^{-1/18}$. (b) The relation (2.4) has solutions corresponding to growing waves directed inside the wave-Mach cone. (c) Solution of the dispersion relation (2.4) for the growth rate $(-\alpha_i)$ of 2D disturbances in a subsonic ($\bar{m} < 0$) or a supersonic ($\bar{m} > 0$) free stream. (d) Solutions of the system (2.12a, b) at times $T = 0.6$, 1.2, 1.8. Here $\bar{m} = -1$ and the forcing is a wall displacement equal to $10(X+3)T\exp[-(X+3)^4 - T^2]$. A wave packet is seen to travel downstream away from the disturbance location.

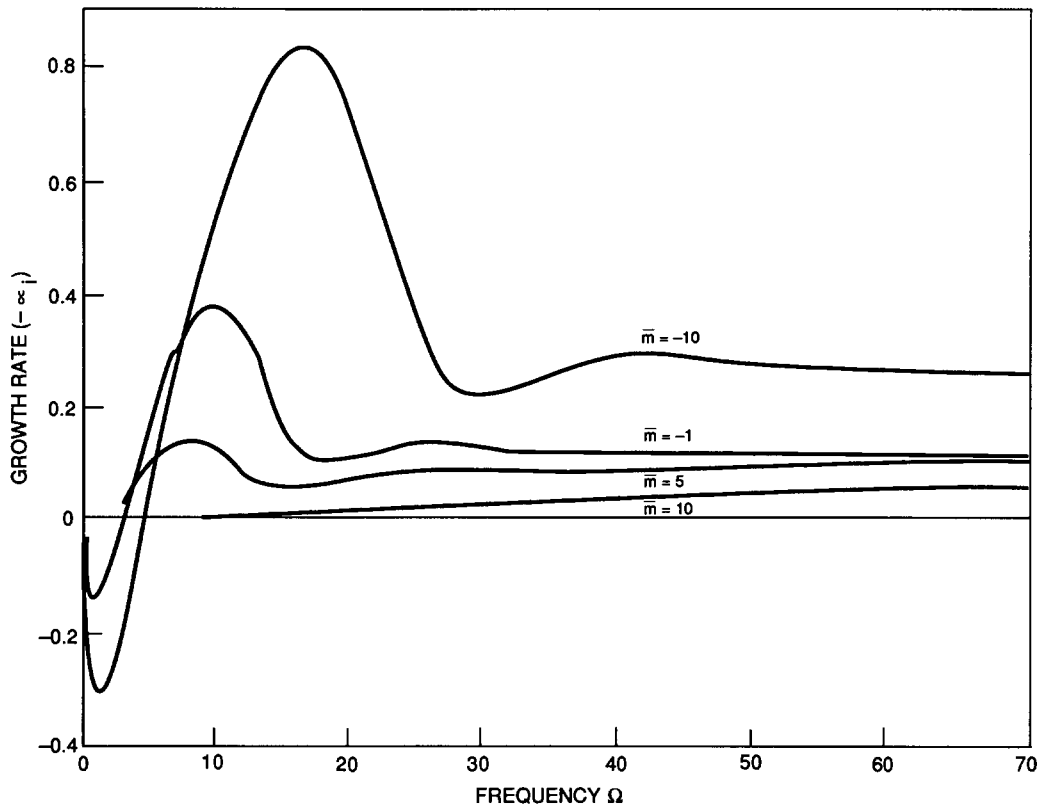

Fig. 1(c). Two-dimensional growth rates vs Ω from Equation (2.4), $\beta^2 = 0$.

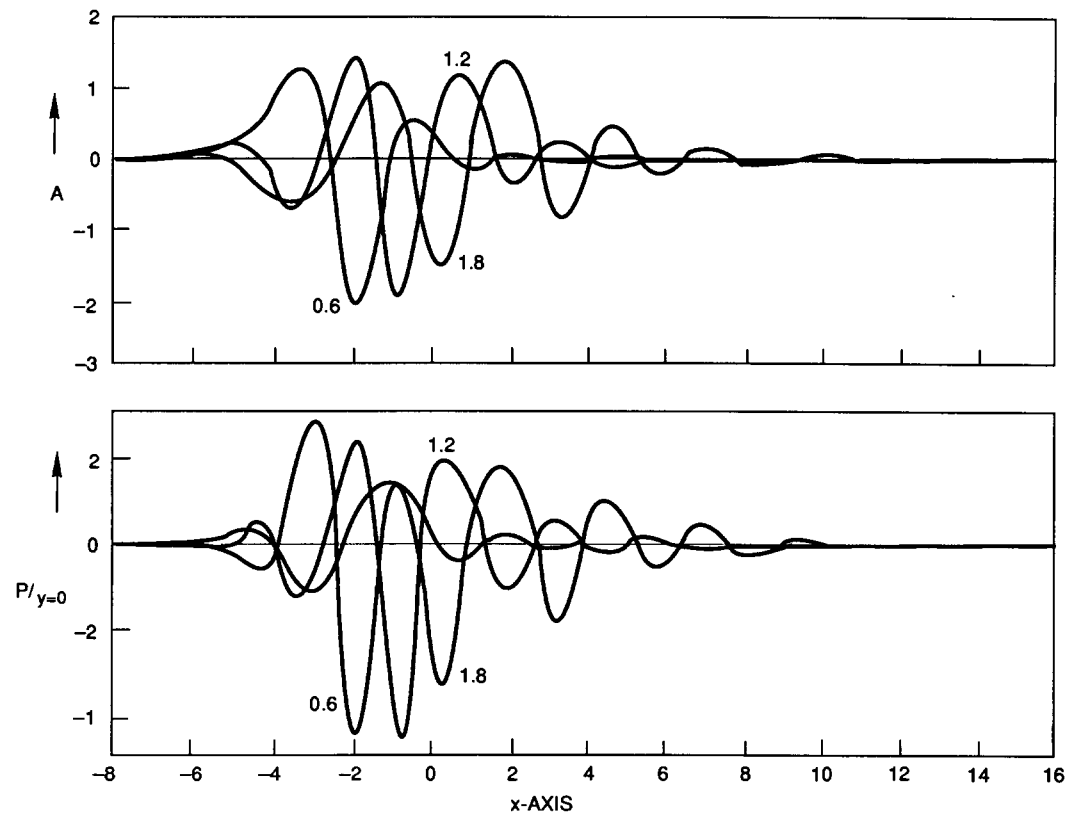

lies just outside the boundary layer. The b_n are $O(1)$ constants, specifically $b_n = C^q(T_w/T_\infty)'\lambda^s$, with C being the Chapman constant in the viscosity-temperature law, λ is the local skin-friction factor, T_w/T_∞ is the local temperature ratio, and $q = \frac{1}{3}, \frac{2}{9}, \frac{11}{18}, \frac{5}{18}, \frac{1}{9}, \frac{7}{18}, \frac{2}{9}, r = \frac{4}{3}, \frac{8}{9}, \frac{13}{9}, \frac{10}{9}, \frac{4}{9}, \frac{5}{9}, -\frac{1}{9}, s = -\frac{4}{3}, -\frac{14}{9}, -\frac{7}{9}, -\frac{13}{9}, \frac{2}{9}, \frac{7}{9}, \frac{4}{9}$, for $n = 1$ to 7 in turn (see Fig. 1). Moreover, this transonic stage has

$$(M_\infty^2 - 1) = Re^{-1/9} b_5 \bar{m} , \tag{2.2}$$

with $\bar{m}$ typically of order unity. In consequence the Navier–Stokes equations reduce to the viscous-inviscid interaction system consisting of the unsteady boundary-layer equations,

$$U_X + V_Y + W_Z = 0 , \tag{2.3a}$$

$$U_T + UU_X + VU_Y + WU_Z = -P_X + U_{YY} , \tag{2.3b}$$

$$W_T + UW_X + VW_Y + WW_Z = 0 + W_{YY} , \tag{2.3c}$$

with

$$U = V = W = 0 \text{ at } Y = 0 \quad \text{and} \quad U \sim Y + A, \quad W \to 0, \text{ as } Y \to \infty \tag{2.3d}$$

(for no slip and matching to the main deck), coupled with the unsteady linearized TSP (Transonic Small Perturbation) equation

$$\bar{m}\bar{P}_{XX} - \bar{P}_{ZZ} + 2\bar{P}_{XT} = \bar{P}_{\bar{y}\bar{y}} , \tag{2.3e}$$

subject to

$$\bar{P} \to 0 \text{ as } \bar{y} \to \infty \quad \text{and} \quad \bar{P} \to P, \quad \bar{P}_{\bar{y}} \to A_{XX}, \text{ as } \bar{y} \to 0 . \tag{2.3f}$$

Here, in scaled terms, $-A$ is the unknown displacement caused by the disturbance in the boundary layer, while P, $\bar{P}$ are the unknown wall pressure and external pressure respectively, and P, A depend on X, Z, T, with U, V, W dependent on X, Y, Z, T. The constraints in (2.3f) ensure the matching with the oncoming stream and between the upper and main decks, in turn. The main novel features in this regime are the unsteady contribution in the outer TSP balance (2.3e), the insignificant transverse pressure gradient in (2.3c), and the property that any waves produced for $\bar{m} > 0$ (see below) can be directed close to the wave-Mach cone which is narrow of characteristic angle $O(Re^{-1/18})$, from (2.1a).

Interest centers, then, on the nonlinear system (2.3). In preparation for the nonlinear analysis below, it is noteworthy that linearization, for small disturbances $\sim \exp\{i(\alpha X + \beta Z - \Omega T)\}$, leads from (2.3) to the eigenrelation

$$\alpha^2 (i\alpha)^{1/3} (k/Ai')(\xi_0) = (2\Omega\alpha + \beta^2 - \bar{m}\alpha^2)^{1/2} \tag{2.4}$$

between the frequency Ω and the wavenumbers α, β. Here the real part of the right-hand side must be positive, $k \equiv \int_{\xi_0}^{\infty} Ai(q)\, dq$ and the argument of $\xi_0 \equiv -i^{1/3}\Omega/(\alpha)^{2/3}$ lies between $-\pi/3$ and $\pi/3$ (see Fig. 1). Further, for high frequencies Ω, in the 2D case $\beta = 0$ say, (2.4) yields the behaviour

$$\alpha \sim \Omega^{3/5}\tilde{\alpha}\left\{1 - \frac{(1+\mathrm{i})\tilde{\alpha}(2-\tilde{\alpha}m)}{2^{1/2}\Omega^{9/10}(5-\tilde{\alpha}m)}\right\}, \tag{2.5a}$$

where

$$m \equiv \Omega^{-2/5}\bar{m}\,, \qquad \tilde{\alpha}m < 2 \quad \text{and} \quad \tilde{\alpha}^3 = \{(2-\tilde{\alpha}m)\tilde{\alpha}\}^{1/2}\,. \tag{2.5b}$$

This acts as a guide for the following nonlinear theory, where it is assumed that W in (2.3) is identically zero (we expect that for many flows w is only $O(\mathrm{Re}^{-3/18})$) with any three-dimensionality entering then through the Z-dependence in the TSP equation (2.3e). We note in passing that the alternative of high-wavenumber focussing via (2.5a) is mentioned in Ref. 33 for linear waves, similar to that in Ref. 34. In the nonlinear framework this would presumably lead on instead to the finite-time break-up of Refs. 17, 34, as an alternative to what follows.

2.2. Nonlinear high-frequency response

The nonlinear unsteady transonic-flow properties are considered now for relatively high frequency since such frequencies, and the corresponding short-scale waves, have been shown (Refs 22, 25) to reflect part of the natural transition process in incompressible boundary layers. The relative Mach number $\bar{m}$ is scaled with $\Omega^{2/5}$ as indicated by (2.5), with $\Omega \equiv |\partial_T|$ being large, which preserves the temporal-spatial balance in (2.3e), and we concentrate on the 2D case $W = \partial_z \equiv 0$ as a starting point, granted that 3D effects are usually strong in transition. The slow spatial growth of order $\Omega^{-3/10}$ suggested by (2.5) can then balance a weak nonlinear effect if the pressure size P is typically of order $\Omega^{7/20}$. Hence this nonlinear regime has the multiple-scale expansion

$$[U, V, P, A] = [\varepsilon(u_0 + \varepsilon^9 u_1 + \varepsilon^{18}u_2),\ \varepsilon^{-1}(v_0 + \cdots),\ \varepsilon^{-7}(P_0 + \cdots),\ \varepsilon(A_0 + \cdots)] + \cdots, \tag{2.6a}$$

$$\partial_X \to \varepsilon^{-12}[\partial_{X_0} + \varepsilon^9 \partial_{X_1} + \varepsilon^{18}\partial_{X_2} + \cdots]\,, \qquad \partial_T \to \varepsilon^{-20}[\partial_{t_0} + \varepsilon^9 \partial_{t_1} + \varepsilon^{18}\partial_{t_2} + \cdots]\,, \tag{2.6b}$$

with $\varepsilon = \Omega^{-1/20}$ small, and $\bar{y} = \varepsilon^{16}y$, $Y = \varepsilon^{10}Y$, while $\bar{m} = \Omega^{2/5}m$ is large positive (supersonic) or negative (subsonic). The resulting properties are summarized as follows.

At leading order, substitution into (2.3) yields solutions of the form

$$P_0 = P_{01}E + \text{c.c.}\,, \qquad E \equiv \exp[\mathrm{i}(\tilde{\alpha}X_0 - t_0)]\,, \tag{2.7}$$

and similarly for U_0, V_0, A_0, where the wave E contains all the fast X_0-, t_0-dependence, P_{01} etc. remain undetermined, and the quasi-inviscid eigenrelation (2.5b) is obtained, as expected.

At second order, the nonlinearity causes harmonics and mean-flow corrections to be induced, along with additional fundamental waves, such that

$$P_1 = P_{12}E^2 + \text{c.c.} + P_{1m} + P_{11}E + \text{c.c.} \tag{2.8}$$

and so on. Here P_{12} etc. can be determined in terms of P_{01}, e.g. $P_{12} = -\tilde{\alpha}^2 P_{01}^2$, $A_{12} = -\tilde{\alpha}^3 P_{01}^2/2$, whereas the extra fundamental leads to the linear equation

$$\partial P_{01}/\partial t_1 + c_g \partial P_{01}/\partial_{X_1} = 0\,, \tag{2.9}$$

indicating that the unknown pressure amplitude P_{01} travels at the group velocity $c_g \equiv (2\tilde{\alpha}^5 + 1)/(\tilde{\alpha}^6 + \tilde{\alpha})$ in the X_1–t_1 frame. This velocity, we note, increases like $\tilde{\alpha}^{-1}$ for small $\tilde{\alpha}$.

At third order, we then obtain the following Ginzburg–Landau equation for the nonlinear development of the high-frequency distribution P_{01}:

$$(1+\sigma)\frac{\partial P_{01}}{\partial t_2} - \mathrm{i}\frac{f(\sigma)}{\tilde{\alpha}^2}\frac{\partial^2 P_{01}}{\partial X_1^2} = \frac{\tilde{\alpha}(1-\mathrm{i})}{2^{1/2}} P_{01} - \frac{5\mathrm{i}}{2}\tilde{\alpha}^4 P_{01}|P_{01}|^2\,, \tag{2.10a}$$

where

$$\sigma \equiv \tilde{\alpha}^{-5} \quad \text{and} \quad f(\sigma) = 1 + \frac{(\sigma/2-1)\sigma}{(1+\sigma)^2}\,. \tag{2.10b}$$

In (2.10a) the linear growth term on the right is due to viscous effects from the Stokes layer and the cubic nonlinear contribution comes partly from harmonic forcing and partly from the mean-flow correction. Mach-number dependence is present via the m–$\tilde{\alpha}$ relation (2.5b), and the term f is always positive, as $\sigma > 2$ from (2.5), with the case $\sigma \to 2+$ corresponding to small $|m|$, i.e. to $|\bar{m}|$ less than the order $\Omega^{2/5}$. Since the cubic coefficient is pure imaginary, (2.10a) is therefore a scaled version of the nonlinear equation for the incompressible case studied in Ref. 20, where it is shown that the wave packet grows in amplitude and spreads spatially in an exponential fashion with amplitude $|P_{01}| \sim \exp(2^{1/2}t_2/3)$ and typical X_1-scale $\sim\exp(2^{1/2}t_2/3)$ downstream at large times. This gives the perhaps surprising result that no qualitative difference from the incompressible regime is found as yet (cf. below).

The amplitude growth far downstream leads however to the distinct nonlinear regime studied next.

2.3. Higher amplitudes

The next regime implied downstream has increased pressure amplitude, with

$$[U, V, P, A] \sim [\Omega^{2/5}, \Omega^{1/2}, \Omega^{4/5}, \Omega^{2/5}]\,, \tag{2.11a}$$

$$[\partial_X, \partial_T, \partial_Y, \partial_{\bar{y}}] \sim [\Omega^{3/5}, \Omega, \Omega^{1/2}, \Omega^{4/5}]\,, \tag{2.11b}$$

and again $\bar{m} \sim \Omega^{2/5}$. These scales correspond to most of the boundary-layer properties becoming fully nonlinear but inviscid, so that in effect (2.3b) holds with the U_{YY} term omitted, while the uniform shear term in (2.3d) is also absent. A solution then is simply $U \equiv A$, which leads to the momentum balance

$$A_T + AA_X = -P_X\,. \tag{2.12a}$$

This is coupled with the TSP response (2.3e, f), which can be written in the integral form

$$P_X = \frac{1}{2^{3/2}\pi}\int_{-\infty}^{T}\int_{-\infty}^{\bar{X}} \frac{A_{ss}(s,\hat{t})\,\mathrm{d}s\,\mathrm{d}\hat{t}}{(T-\hat{t})^{1/2}(\bar{X}-s)^{3/2}}\ [\bar{X} \equiv X - \bar{m}(T-\hat{t})/2] \tag{2.12b}$$

to provide two equations, (2.12a, b), controlling P, A. As in the incompressible cases studied in previous works, vorticity bursting from the nonlinear viscous sublayer near the wall, where Y is $O(\Omega^{-1/2})$, is likely to occur especially for severe gradients A_X and forms an important extra ingredient in the nonlinear transition process, but again, as a first step, the bursting is neglected here.

The present nonlinear system (2.12a, b) is a transonic counterpart of the Benjamin–Ono and Burgers equations holding in the pure subsonic and supersonic cases respectively (Ref. 22), but it is distinct in that the pressure-displacement law (2.12b) is not quasi-steady. Those pure subsonic and supersonic nonlinear cases are stable and indeed can be obtained as special limits of the present system; for example, simple traveling-wave solutions of (2.12a, b) dependent upon $(X - cT)$ are governed either by the Benjamin–Ono form

$$(A - c)A_X = \frac{-(2c - \bar{m})^{-1/2}}{\pi} \int_{-\infty}^{\infty} \frac{A_{ss}(s)\,ds}{(X - s)}\,, \tag{2.13a}$$

for relative *subsonic* flow where $(2c - \bar{m}) > 0$, or by the Burgers form

$$(A - c)A_X = |2c - \bar{m}|^{-1/2} A_{XX} \tag{2.13b}$$

in relative *supersonic* flow where $(2c - \bar{m}) < 0$. The appropriate solutions then are always smooth, even though severe gradients can develop. A similar match-up for non-simple waves can be verified at relatively large positive or negative m values. The full properties of (2.12a, b), in contrast, are unknown and require numerical investigation, there being particular interest in the possibility (suggested by an order-of-magnitude argument) that finite-time singularities may develop in this transonic regime. A computational study of the fully nonlinear problem is under way (see also Fig. 1).

2.4. The Euler stage, and further comments

At larger $|\bar{m}|$ the flow enters the pure subsonic or supersonic regime and larger disturbances are needed if the fully nonlinear responses are to be maintained. This can be checked as follows. In the nonlinear inviscid transonic stage of (2.12) $\bar{m}$ (or m) can be factored out by scaling P, A, X, $\bar{y}$, T with $\bar{m}^2$, $\bar{m}$, $\bar{m}^{-3/2}$, $\bar{m}^{-2}$, $\bar{m}^{-5/2}$ respectively. So, e.g., the streamwise length scale becomes $O(\mathrm{Re}^{-3/9}\bar{m}^{-3/2})$, from (2.1), and that shortens to the boundary-layer scale $O(\mathrm{Re}^{-1/2})$ when $\bar{m}$ reaches $O(\mathrm{Re}^{1/9})$, which is exactly when $|\mathrm{M}_\infty - 1|$ becomes $O(1)$ in view of (2.2). Simultaneously the typical upper-deck extent $\mathrm{Re}^{-5/18}\bar{m}^{-2}$ reduces to $\mathrm{Re}^{-1/2}$, the same scale, and the velocities u, v and the pressure variation p all increase to $O(1)$.

Hence an extension of (2.3) to pure subsonic or supersonic flow points to the compressible Euler stage, of increased amplitudes and faster spatial and temporal variation, with the unsteady nonlinear Euler system

$$\varrho_t + (\varrho u)_x + (\varrho v)_y = 0\,, \tag{2.14a}$$

$$\varrho(u_t + uu_x + vu_y) = -p_x\,, \tag{2.14b}$$

$$\varrho(v_t + uv_x + vv_y) = -p_y\,, \tag{2.14c}$$

$$\varrho(p_t + up_x + vp_y) = \gamma p(\varrho_t + u\varrho_x + v\varrho_y)\,, \tag{2.14d}$$

$$(u, v, \varrho, p) \to (1, 0, 1, \gamma^{-1}M_\infty^{-2}) \text{ as } y \to \infty, \tag{2.14e}$$

$$v = 0 \text{ at } y = 0 \tag{2.14f}$$

holding across the boundary layer, x, y, t all being scaled on $\mathrm{Re}^{-1/2}$ and $|M_\infty - 1|$ being $O(1)$. This nonlinear unsteady system tends to that in Section 2.3 as $M_\infty \to 1\pm$, as expected. It is of further interest because it also captures the nonlinear versions of compressible inviscid modes, for which only linear theory, e.g. Refs 35 and 36, has been studied hitherto (apart from the present work and studies by Dr J.S.B. Gajjar), and nonlinear inflexional modes due to an adverse external pressure gradient are also incorporated.

The same Euler stage is encountered if the input frequency Ω in Sections 2.2 and 2.3 is raised to the order $\mathrm{Re}^{5/18}$, since $\bar{m}$ is scaled with $\Omega^{2/5}$ and therefore increases again to $O(\mathrm{Re}^{1/9})$. Moreover, viscous sublayer bursting is again likely, analogous to that described in Section 2.3. The major points, however, are these: first, there is no clear sign yet of transition occurring more readily in the transonic regime than in pure subsonic or supersonic flow, in contrast with the next two sections; second, the transonic regime of Sections 2.2 and 2.3 may provide an analytical and more understandable guideline to the nonlinear unsteady response in the Mach-number range of practical concern. A third point here concerns *nonparallel-flow* effects, due for instance to shock-wave/boundary layer interaction and/or flow separation. These effects are relatively small in the situations addressed so far (cf. below however), due to the short length scales involved, and they can be encompassed as secondary effects in the manner of Refs 20, 22, 26. We find that the resulting growth rate in the transonic regime is given by

$$G_r = \Omega^{-3/10}\left\{2^{1/2}\tilde{\alpha} - 2|m|^{1/4}\frac{\mathrm{d}\bar{A}}{\mathrm{d}X}\left(1 + \frac{f(\sigma)}{(2+\sigma)}\right)\right\}\frac{\tilde{\alpha}}{2(2+\sigma)}, \tag{2.15}$$

where the first contribution in curly parentheses is the viscous one (as in (2.5)) whereas the second contribution gives the nonparallel effect from a basic flow with displacement $-\bar{A}(X)$. As in the incompressible case, therefore, an increasing displacement where $-\mathrm{d}\bar{A}/\mathrm{d}X$ is positive produces an extra destabilizing effect, e.g. in breakaway separating flow ($-\mathrm{d}\bar{A}/\mathrm{d}X \to \infty$) the destabilization increases dramatically downstream (see also Refs 23, 26). This ties in with the effects of separation studied in Section 3. Finally, the connections are noted with Appendix A below, at large $\bar{m}$ in effect, with the alternate high-frequency range studied in Appendix C, and with the transonic stage II addressed in the next section, as well as with the 3D properties in Section 4.

3. The transonic regime II

The flow structure in this regime II is for local Mach numbers closer to unity than in I. Like I the present stage can incorporate *separation* in the boundary layer, a strong destabilizing influence, but in contrast with I the present regime is able also to incorporate directly the presence of an external *shock* impinging on the boundary layer, by virtue of the nonlinearity in the flow just outside the boundary layer (see also Fig. 2). In what follows, the interactive flow structure is summarized in Sub-Section 3.1, its small-disturbance properties are considered in 3.2 for non-separating motion, and then 3.3 deals with the effects of separation and shock oscillation.

3.1. The interactive flow structure

The current flow structure at large Reynolds numbers holds for both 2D and 3D flows, at Mach numbers M_∞ of size $1 + O(Re^{-1/5})$, and the flow solution has the form

$$[x - x_0, z - z_0, t] = [Re^{-3/10} b_1 X, Re^{-1/5} b_2 Z, Re^{-1/10} b_3 T], \tag{3.1a}$$

$$y = Re^{-3/5} b_4 Y \text{ (lower deck)}, Re^{-1/5} b_2 \bar{y} \text{ (upper deck)}, \tag{3.1b}$$

$$[u, v, w, p - p_\infty] = [Re^{-1/10} b_5 U, Re^{-2/5} b_6 V, Re^{-1/10} b_5 b_2 b_1^{-1} W, Re^{-1/5} b_7 P], \tag{3.1c}$$

where the order-one constants b_n, for $n = 1$ to 7, are as in Section 2 except that $q = \frac{3}{10}, \frac{1}{5}, \frac{1}{10}, \frac{3}{5}, \frac{1}{10}, \frac{2}{5}, \frac{1}{5}$, $r = \frac{3}{2}, \frac{3}{2}, \frac{3}{2}, \frac{3}{2}, \frac{1}{2}, \frac{1}{2}, 0$, $s = -\frac{7}{5}, -\frac{8}{5}, -\frac{9}{5}, -\frac{4}{5}, \frac{1}{5}, \frac{4}{5}, \frac{2}{5}$, respectively. Again, (3.1c) applies for the lower-deck flow, while in the upper deck just exterior to the boundary layer the normalized velocity potential is given by

$$\phi = x + Re^{-1/2} b_1 b_7 \bar{\phi}, \tag{3.2}$$

and the Mach number satisfies

$$M_\infty^2 - 1 = Re^{-1/5} b_7 \tilde{m} \tag{3.3}$$

with $\tilde{m}$ being typically $O(1)$. The resulting governing equations for this regime II are the quasi-steady boundary-layer equations holding near the surface,

$$U_X + V_Y + W_Z = 0, \tag{3.4a}$$

$$UU_X + VU_Y + WU_Z = -P_X + U_{YY}, \tag{3.4b}$$

$$UW_X + VW_Y + WW_Z = 0 + W_{YY}, \tag{3.4c}$$

subject to

$$U = V = W = 0 \text{ at } Y = 0 \quad \text{and} \quad U \sim Y + A, \quad W \to 0, \text{ as } Y \to \infty, \tag{3.4d}$$

interacting with the unsteady nonlinear TSP equation which controls the upper-deck properties:

$$\bar{\phi}_{\bar{y}\bar{y}} + \bar{\phi}_{ZZ} = [\tilde{m} + (\gamma + 1)\bar{\phi}_X]\bar{\phi}_{XX} + 2\bar{\phi}_{XT}, \tag{3.5a}$$

subject to

$$\bar{\phi}_X \to -P, \quad \bar{\phi}_{\bar{y}} \to -A_X, \text{ as } \bar{y} \to 0, \tag{3.5b}$$

and to the appropriate farfield conditions.

We concentrate again on the case of zero spanwise velocity within the boundary layer, $W \equiv 0$, leaving 3D effects to arise only via the nonlinear TSP balance (3.5a). These 3D effects are then addressed for the most part in Section 4 since here the stress is on nonlinear

features, for which the simpler 2D version forms a useful test-bed. It should be remarked also here that the physical balances in (3.4), (3.5), with the lower deck responding quasi-steadily and the upper deck being fully unsteady, but both nonlinear, are distinct from those in the transonic regime I (see (2.3)) and in the pure subsonic and supersonic regimes where full unsteadiness concentrates in the lower-deck balances.

In the current regime controlled by (3.4), (3.5) shocks can occur, depending on the effective Mach number $\tilde{m}$, because of the nonlinear TSP behavior in (3.5a). The steady-flow problem for instance is studied by, among others, Refs 37, 38, the latter including separated-flow situations for sufficiently strong shocks. The shock strength is still sufficiently low however that the potential-flow approximation remains valid. In the present unsteady case the jump conditions across any shock occurring follow from the Rankine–Hugoniot relations and take the form, for 2D motion,

$$\bar{\phi}_1 = \bar{\phi}_2 \,, \tag{3.6a}$$

$$\tilde{m} + \left(\frac{\gamma+1}{2}\right)(\bar{\phi}_{1X} + \bar{\phi}_{2X}) = \bar{G}_{\bar{y}}^2 + 2\bar{G}_T \tag{3.6b}$$

at the shock given by

$$X = \bar{G}(\bar{y}, T) \,. \tag{3.6c}$$

If the shock shape is written instead as $\bar{y} = \bar{F}(X, T)$ then (3.6b) is replaced by $\tilde{m}F_X^2 + 2F_XF_T = 1 - (\gamma+1)F_X^2(\bar{\phi}_{1X} + \bar{\phi}_{2X})/2$. The subscripts 1, 2 refer to the solution values immediately upstream and downstream of the unsteady shock.

The additional conditions on the potential $\bar{\phi}$, in the farfield, are problem-dependent but the constraint $\bar{\phi}_X \to 0$ far upstream is usually relevant and typically $\bar{\phi}_X$ should be negative at downstream infinity due to the shock-induced losses. It is noted that the transformation $\bar{\phi} + \tilde{m}X/(\gamma+1) \to \bar{\phi}$ corresponds simply to a re-definition of the oncoming free-stream speed and pressure, in effect suppressing the $\tilde{m}$ term in (3.5a) and hence the Mach-number dependence. In similar vein, travelling-wave solutions of (3.4), (3.5) with speed c, say, reduce to the steady version mentioned earlier but in a moving frame such that the effective Mach number $\tilde{m}$ is replaced by $(\tilde{m} - 2c)$. So, for example, a *downstream-travelling shock* of positive speed c can render a supersonic portion of the flow ($\tilde{m} > 0$) effectively subsonic if the speed c exceeds $\tilde{m}/2$; conversely, an *upstream-travelling shock*, where $c < 0$, produces effectively supersonic motion (solvable by characteristics) if $|c| > -\tilde{m}/2$, even in a subsonic portion where $\tilde{m} < 0$. This change in type may be significant in terms of the stability and transition characteristics of the boundary layer since these latter characteristics depend on whether the flow is effectively sub- or supersonic.

3.2. Small-disturbance properties (non-separated)

Linearization of the governing equations (3.4), (3.5) about the basic attached-flow state (with $U - Y$ and $\bar{\phi}$ small, compare the next section) leads to the dispersion relation

$$\alpha^2(\mathrm{i}\alpha)^{1/3}/(3Ai'(0)) = (2\Omega\alpha + \beta^2 - \tilde{m}\alpha^2)^{1/2} \tag{3.7}$$

for waves $\sim\exp(\mathrm{i}(\alpha X + \beta Z - \Omega T))$. Here (3.7) merges with the earlier relation (2.4) but

produces only stable disturbances, traveling upstream, for both the super- and sub-critical ranges $\tilde{m} \gtrless 0$.

For the *supersonic* range, $\tilde{m} > 0$, first, the case of zero frequency Ω yields the steady-flow eigenvalue $\alpha = -i\tilde{m}^{3/8}d^{-3/4}r^3$ governing upstream influence in supersonic boundary layers, where $d \equiv [-3Ai'(0)]^{-1} > 0$ and r satisfies $r^{14} - r^6 = d^{3/2}\tilde{m}^{-7/4}\beta^2$. Here 2D disturbances have zero β and hence $r = 1$, whereas 3D disturbances with large β yield $r \sim d^{3/28}\tilde{m}^{-1/8}\beta^{1/7}$ and hence α is then independent of the Mach number, a result which connects with the 3D theory in Section 4.5 below. In unsteady flow, as Ω increases the asymptote $\alpha \sim \exp(-7\pi i/11)(2\Omega/d^2)^{3/11}$ is attained at large Ω, for any β, producing short-wavelength disturbances which travel upstream and decay rapidly.

For the *subsonic* range, second, where $\tilde{m} < 0$, the large-Ω and the large-β-zero-frequency properties are the same as above. For $O(1)$ values of β however the zero-frequency case has $|\tilde{m}|$ replacing $\tilde{m}$ in the formulae for α in the previous paragraph along with a sign change in the r^6 term. In consequence we now have $r \sim d^{1/4}|\tilde{m}|^{-7/24}\beta^{1/3}$ at small β, implying that such upstream influence in steady subsonic motion is possible only for 3D disturbances with "angles" more oblique than $\tan^{-1}(|\tilde{m}|^{1/2})$, cf. the wave-Mach cone in Ref. 21. Further, in the unsteady case of nonzero Ω these subsonic modes are subject to a cut-off, for any β, where the required free-stream decay is lost. Thus if the value of $[\Omega d^{3/4}|\tilde{m}|^{-11/8}/\cos(2\pi/7)]^{1/3}$ lies between the positive roots of $r^{14} - r^6 + d^{3/2}|\tilde{m}|^{-7/4}\beta^2 = 0$ then no waves exist; while outside this range of frequencies Ω the waves that do exist yield only upstream-travelling decaying disturbances again. It is found that there are no such roots if $d^{3/2}|\tilde{m}|^{-7/4}\beta^2 > (5/14)^{3/4} - (5/14)^{7/4}[= 0.297]$. So as the flow becomes locally more subsonic, corresponding to increasingly negative $\tilde{m}$, a wider range of β values becomes cut off.

Given the above stability features of the non-separated flow in this regime II, there is next the issue of whether destabilization, linear or nonlinear, may be provoked either by the presence of a *shock*, or by *separation* due to a sufficiently large pressure rise, or possibly both. The shock effectively splits the streamwise interval into two semi-infinite ones, invalidating the usual normal-mode decomposition, while any separation alters the basic flow and hence its stability characteristics. Both are in addition nonparallel-flow phenomena, and indeed the predictions below concerning the effects of separation are analogous to the nonparallel flow-instability result (2.15), in effect for enhanced separation amplitudes. The shock and the separation effects are tackled in the following sub-section.

3.3. Effects of separation and shock oscillation

The quasi-steady boundary-layer response (3.4) controlling the lower-deck behavior can accommodate *separation* caused by an incident shock (Ref. 38), at least within the limits described subsequently in Section 5. The unsteady small-disturbance properties of such a separating flow, or any grossly disturbed motion which provokes positive boundary-layer displacement, are then of much interest since they are found below to exhibit potential instabilities, as opposed to the pure stability demonstrated for the non-separated flow in the previous section. The *destabilization* can be modelled by the inviscid formulation of Ref. 23 for linearly or nonlinearly disturbed separating flows in which the governing equations are

$$UU_X = -P_X\,, \qquad (SU)_X = 0\,, \qquad (S + A)(S + A)_X = -P_X\,. \tag{3.8a–c}$$

Here $(U, P, S, A)(X, T)$ denote in turn the velocity between the separated shear layer and the surface, the pressure, the shear-layer position and the negative displacement of the

boundary layer, all of which are unknowns, and the system is completed by the pressure-displacement law stemming from the TSP balance (3.5). Small unsteady disturbances of high wavenumber α therefore lead to the boundary-layer response

$$[1 + S_0(S_0 + A_0)/U_0^2]P = -(S_0 + A_0)A \tag{3.9a}$$

from (3.8), the subscript zero standing for the basic separated flow, and the instability of the interactive flow is then dictated by (3.9a) coupled with the TSP relation in 2D,

$$P = \alpha^2[\alpha^2(2c - \tilde{m})]^{-1/2}A \tag{3.9b}$$

from (3.5). Even with significantly disturbed but unseparated motion, where $S_0 \equiv 0$ and $A_0 < 0$, corresponding to a large positive displacement, non-decaying waves exist since then (3.9a, b) yield the dispersion relation

$$\alpha = (-A_0)(2c - \tilde{m})^{1/2} . \tag{3.9c}$$

These neutral waves can travel upstream [for $-|\tilde{m}|/2 < c < 0$] or downstream [$c > 0$] in subcritical motion, and downstream in the supercritical case [$c > \tilde{m}/2$] (see Fig. 2). Other ingredients of separated flow likewise tend to produce destabilization. For example, large-scale eddies with constant vorticity (Ref. 23), rather than zero vorticity as in (3.8), are modelled in the current regime II by the law $P = d_1(T) - \zeta^2 S^2/8$, with $S \approx -A$ and d_1 an undetermined function of time T. So small disturbances are governed by

$$P = \zeta^2 S_0 A/4 , \tag{3.10}$$

and the link with (3.9b) then produces the eigen-relation (3.9c) again but with $\zeta^2 S_0$ replacing $-A_0$, thus again inducing non-decaying waves.

Separation has a similar de-stabilizing effect in the regime I of Section 2, a point taken up later in Section 5.

We turn now to the other major feature uniquely captured by the present regime, shock oscillations or *flutter*. The basic 2D steady upper-deck motion with an overall pressure rise from P_1 to P_2 may be modelled simply by the form $\bar{\phi} = \bar{\phi}_1 = -P_1 X$ for $X < 0$, $\bar{\phi} = \bar{\phi}_2 = -P_2 X$ for $X > 0$, say over a relatively long scale, for a normal shock ($\bar{G} \equiv 0$) at $X = 0$; here the uniform pressures P_1, P_2, satisfy

$$P_1 + P_2 = 2\tilde{m}/(\gamma + 1) \tag{3.11}$$

from (3.6). Small 2D disturbances are therefore controlled by the linearized TSP equations, in which $[\tilde{m} - (\gamma + 1)P_{1,2}]$ replace $[\tilde{m} + (\gamma + 1)\bar{\phi}_X]$ for X negative and positive respectively in (3.5a), and by the linearized shock conditions

$$\bar{\phi}_1 - P_1\bar{G} = \bar{\phi}_2 - P_2\bar{G} , \tag{3.12a}$$

$$\bar{G}_T = \left(\frac{\gamma + 1}{4}\right)(\bar{\phi}_{1X} + \bar{\phi}_{2X}) , \tag{3.12b}$$

at $X = 0\pm$, from (3.6). Oscillatory behavior $\sim \exp(\mathrm{i}\alpha X - \mathrm{i}\Omega T)$, substituted into (3.12a, b), then gives the jump condition

$$\bar{\phi}_2 - \bar{\phi}_1 = -(P_2 - P_1)\frac{(\gamma+1)\alpha}{2\Omega}(\bar{\phi}_2 + \bar{\phi}_1)\,, \tag{3.13a}$$

on elimination of $\bar{G}$. So natural oscillations on the downstream (2) side have a wavespeed $c = \Omega/\alpha$ which is negative, given by

$$c = -(\gamma+1)(P_2 - P_1)/4\,, \tag{3.13b}$$

if the upstream-side disturbance potential $\bar{\phi}_1$ is assumed known. The latter potential has a natural oscillation speed of $-c$, i.e. positive, at the shock, although a more significant property on the upstream supersonic side is the decay rate of the unsteady disturbances as given earlier in Sub-Section 3.2, which does indeed help to fix the upstream interactive solution $\bar{\phi}_1$ as a single-wave form. The downstream solution $\bar{\phi}_2$ can then also be determined in principle, e.g. by use of characteristics or spatial transforms if the flow there is super- or sub-critical respectively, coupled with the $P - A$ response due to the boundary layer. The most intriguing feature there, however, is that the downstream-side flow solution "blows up" if the wavespeed c of the small disturbances downstream ever matches that of the shock oscillations in (3.13b), i.e. a *resonance* occurs. Such a resonance cannot arise for unseparated motion as that motion cannot support neutral waves anyway (see Sub-Section 3.2). But resonance can set in for separated motion since its dispersion relation (3.9c) does allow neutral waves with negative c, as Fig. 2 shows, in the sub-critical range.

The criterion for resonance between the shock flutter and the separation instabilities, then, is given by (3.9c) combined with (3.13b) (see Fig. 2). This is for a normal impinging shock in

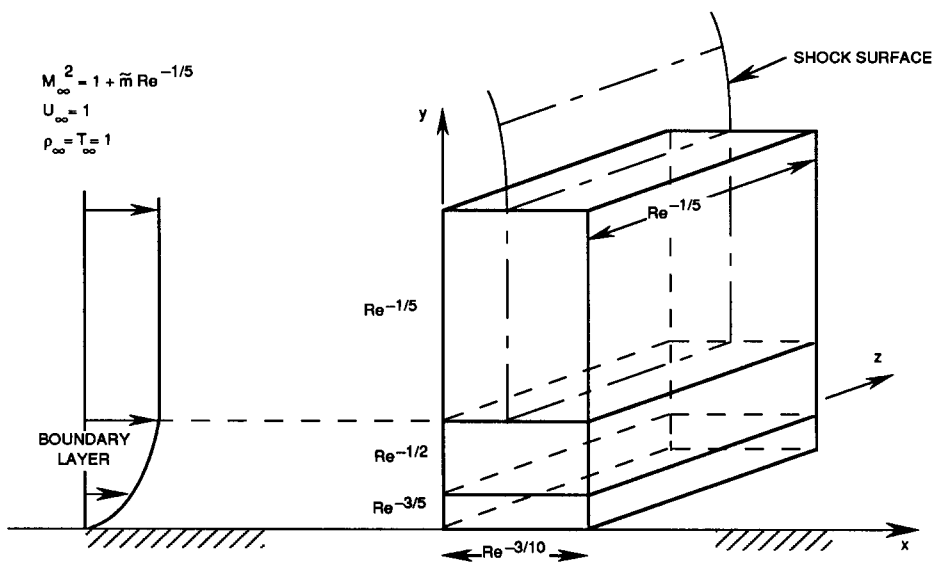

Fig. 2(a). Disturbance structure.

Fig. 2. (a) Nonlinear disturbance structure for regime II where $M_\infty^2 - 1 = O(Re^{-1/5})$. A 2D flow is subjected to a 3D disturbance of small, $O(Re^{-1/10})$, angle to the oncoming flow. This disturbance can interact with a shock present in the flow; the shock surface is effective only in the free stream. (b) The mechanism for unsteady shock/boundary-layer interaction causing self-sustaining shock flutter. Motion of the shock downstream causes it to increase in strength. The boundary layer separates or thickens substantially and undergoes transition, the shock strength is reduced and the shock moves upstream. (c) Neutral waves on a disturbed boundary layer (displacement $= -A_0 > 0$), in regime II, for supercritical ($\tilde{m} > 0$) and subcritical ($\tilde{m} < 0$) flow.

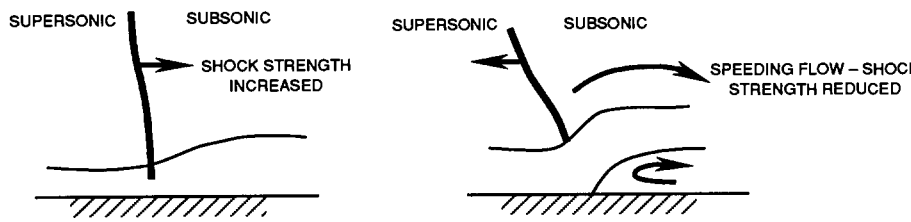

Fig. 2(b). Unsteady shock/boundary-layer interaction.

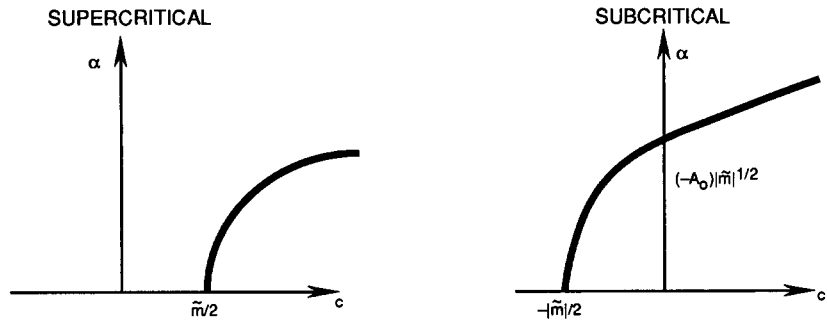

Fig. 2(c). Neutral waves in a disturbed boundary layer.

2D flow. An oblique shock is found to yield a modified version of (3.13b) which allows downstream-travelling oscillations if the obliqueness is sufficiently pronounced, and 3D effects (see Section 4) can also modify both (3.13b) and (3.9c). Nevertheless, the predicted resonance in the simpler model above seems to provide a potentially powerful trigger for transonic transition to take place; with that in mind, we are conducting computational studies of the full nonlinear TSP system (3.5) interacting with the boundary layer (3.4), including the linearized version of Ref. 37 for weaker shocks and no separation as well as the typical nonlinear inviscid version where $P = -A^2/2$ as implied by (3.8), (3.9).

4. Three-dimensional transition properties

With the 2D theory above having established some of the main transonic scales and viscous-inviscid interactions occurring, we move on here to describe certain of the extra 3D effects arising in transonic transition. It turns out that these effects can be especially powerful compared with the 2D effects and they also exhibit a number of nonlinear features peculiar to the transonic range (see Figs 3–5). Again a start is made with the transonic regime I defined by (2.2), in Sub-Sections 4.1–4.3, for high frequencies, followed by remarks on the regime II in Sub-Section 4.4, while 4.5 addresses additional 3D transonic interactions of both the viscous-inviscid kind and the vortex-wave type. All these 3D flow features are in addition to and distinct from the previous 2D ones in the sense that they are not merely passive extensions of the 2D cases. It remains to be seen whether the 3D extension of the separation-induced properties studied in Section 3 also produces distinct flow features; here we focus more on the possible non-separated transonic transition processes in 3D, finding in particular some substantial differences between the linear and nonlinear predicted behavior.

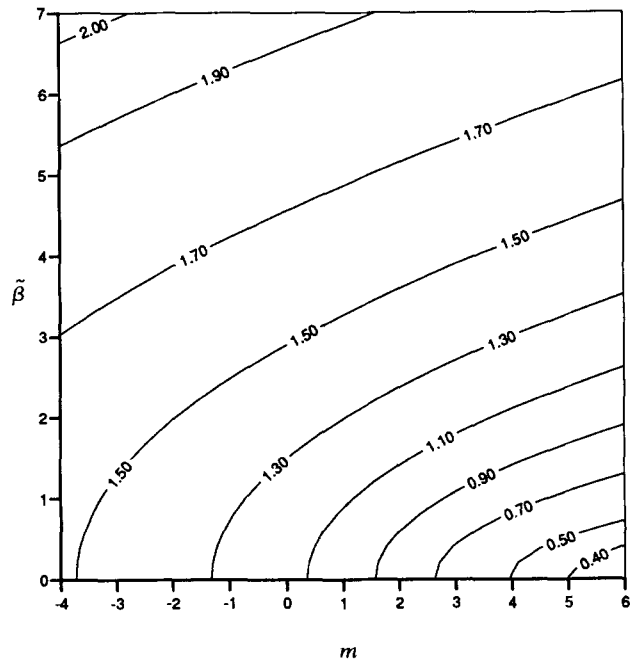

Fig. 3(a). A contour plot in $(m, \tilde{\beta})$ space of curves of constant spanwise wave number $\tilde{\alpha}$, in the 3D high-frequency limit.

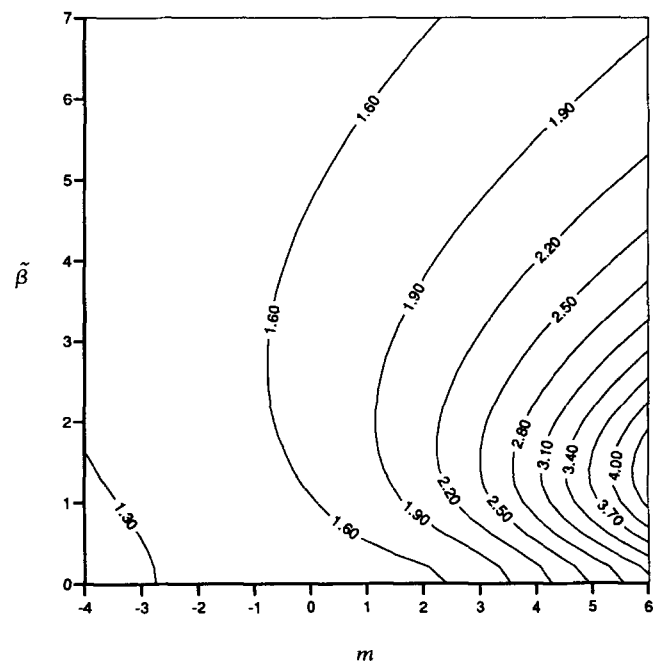

Fig. 3(b). A contour plot in $(m, \tilde{\beta})$ space of curves of constant scaled group velocity in the x-direction, $c_{gx} = \frac{1}{\tilde{\alpha}}\left(\frac{3\tilde{\alpha}^5 - 1 + m\tilde{\alpha}}{\tilde{\alpha}^5 + 1}\right)$, in the 3D high-frequency limit.

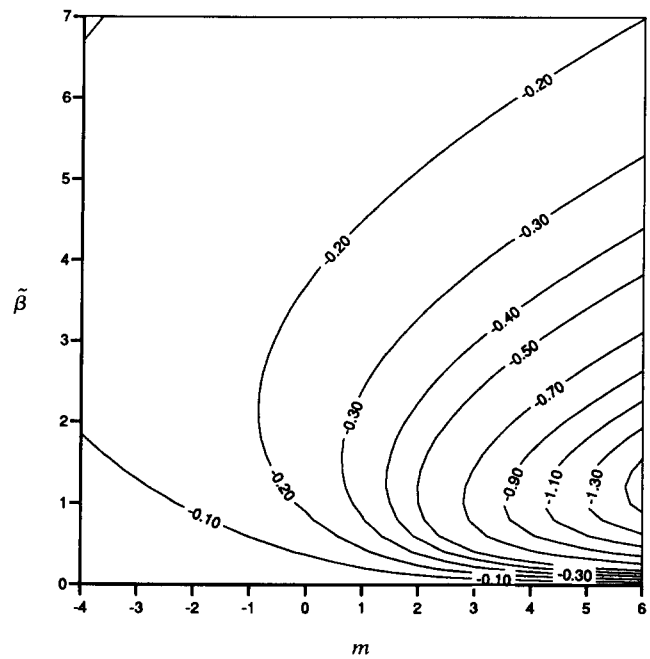

Fig. 3(c). A contour plot in $(m, \tilde{\beta})$ space of curves of constant scaled group velocity in the z-direction, $c_{gz} = -\frac{1}{\tilde{\beta}}\left(\frac{\tilde{\beta}^2}{\tilde{\alpha}^6 + \tilde{\alpha}}\right)$, in the 3D high-frequency limit.

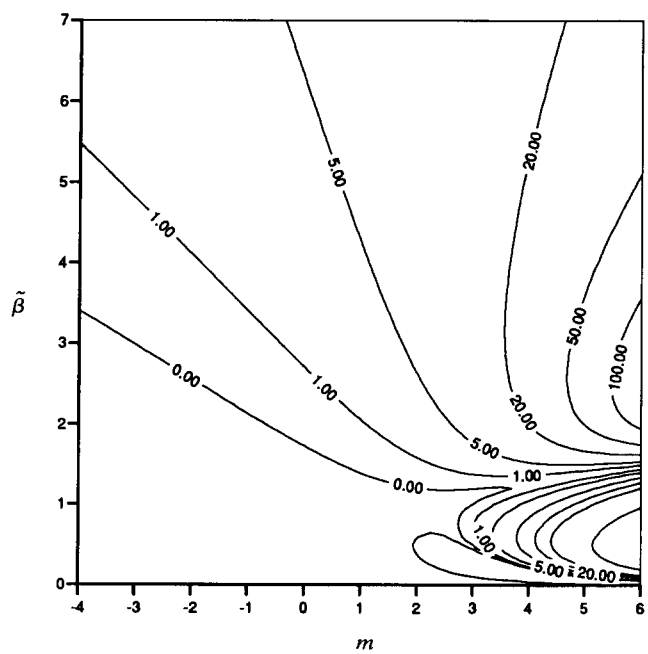

Fig. 3(d). A contour plot in $(m, \tilde{\beta})$ space of curves of constant $\hat{A}\hat{H}\hat{B}^2 = \hat{A}(4\hat{A}\hat{C} - \hat{B}^2)$. If this quantity is positive the dispersive term in (4.9) leads to spreading and growth like $\exp(2\hat{T}/3)$. If it is negative it leads to focussing and more rapid growth like $\exp(2\hat{T})$.

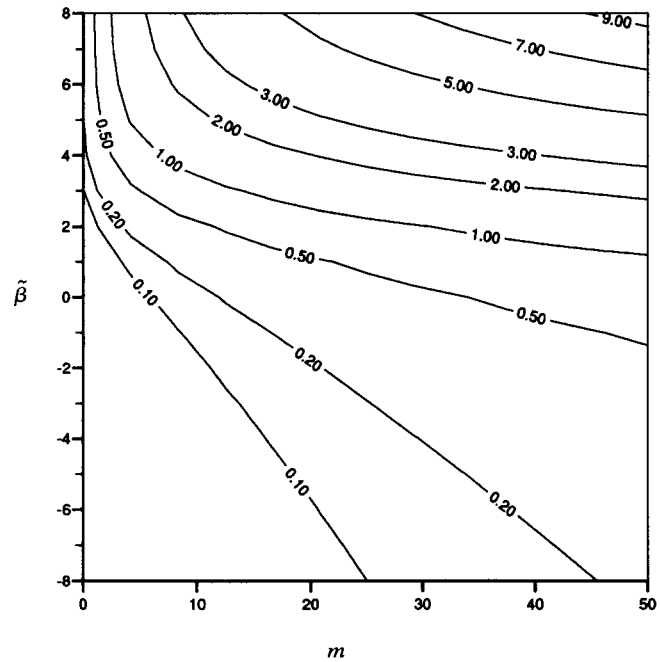

Fig. 4. (a) A contour plot in (m, β) space of curves of constant μ satisfying (4.15a–d).

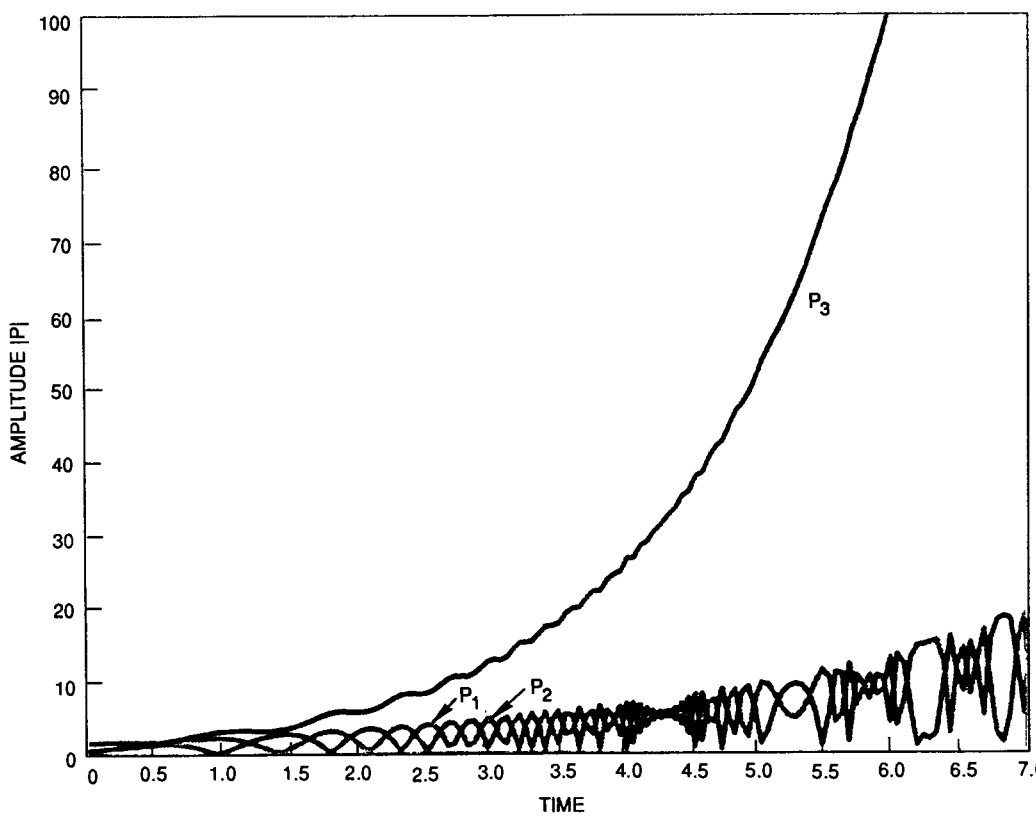

Fig. 4. (b). A computational solution of the triad system (4.18a–c).

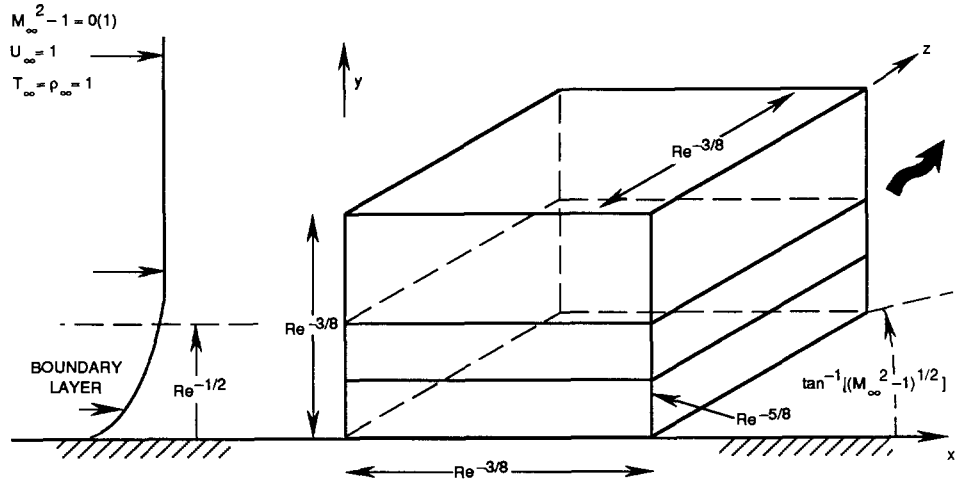

Fig. 5. Nonlinear disturbance structure for the 3D major modes. Waves are directed outside of the wave-Mach cone, which makes an $O(1)$ angle with the oncoming flow.

4.1. *Linear 3D properties (regime I)*

At high frequencies Ω in the governing system (2.3) it can be seen that 3D modes have the greatest growth rates, according to linear theory, since the 3D extension of the dispersion relation (2.5) is

$$\alpha \sim \Omega^{3/5}\alpha_0\left[1-\left(\frac{1+\mathrm{i}}{2^{1/2}}\right)\frac{\Omega^{-9/10}\tilde{\alpha}_0^7}{2\tilde{\alpha}_0^6+\tilde{\alpha}_0+\tilde{\beta}^2}+\cdots\right] \tag{4.1a}$$

where now

$$\tilde{\alpha}_0^3=(2\tilde{\alpha}_0+\bar{\beta}^2-m\tilde{\alpha}_0^2)^{1/2}\,, \tag{4.1b}$$

$\bar{m}=\Omega^{2/5}m$ again and $\partial_Z=\mathrm{i}\Omega^{4/5}\tilde{\beta}$ defines $\tilde{\beta}$. Thus for relatively strong 3D dependence, i.e. as $\tilde{\beta}\to\infty$, $\tilde{\alpha}_0$ grows like $\tilde{\beta}^{1/3}$ and so the spatial growth rate

$$-\alpha_i \sim \Omega^{-3/10}\tilde{\beta}^{2/3}/(2^{1/2}3) \tag{4.2}$$

also increases with increasing $\tilde{\beta}$.

We observe that the expansion above alters when $\tilde{\beta}$ is as large as $\Omega^{7/2}$, with α then $O(\Omega^{3/2})$ and ξ_0 becoming $O(1)$, although the result (4.2) is retrieved still at relatively large frequencies. Again, if $\bar{m}$ remains of size $\Omega^{2/5}$ there is a merging with the so-called minor mode of Ref. 19, while at larger relative Mach numbers $\bar{m}$ of order $\Omega^{22/5}$ the merging with the major mode is achieved.

More significantly, however, the group velocity c_{gZ} associated with the spanwise dependence is in the direction opposite to that of the phase velocity, since

$$c_{gX}=\left(\frac{6-A_0-2C_0}{2+A_0}\right)\tilde{\alpha}^{-1}\,,\qquad c_{gZ}=-\left(\frac{2B_0}{2+A_0}\right)\tilde{\beta}^{-1}\,. \tag{4.3}$$

Here $A_0 = 2\tilde{\alpha}^{-5}$, $B_0 \equiv \tilde{\beta}^2\tilde{\alpha}^{-6}$, $C_0 = -m\tilde{\alpha}^{-4}$, where the wavenumbers are given by $\partial_{X,Z} = \mathrm{i}(\Omega^{3/5}\tilde{\alpha}, \Omega^{4/5}\tilde{\beta})$ with $\tilde{\alpha}$ positive, and $\partial_T = -\mathrm{i}\Omega$ defines the frequency as before, so that the dispersion relation reads

$$A_0 + B_0 + C_0 = 1 \tag{4.4}$$

For example, if $\tilde{\beta}$ is large, then $B_0 \to 1$ and A_0, C_0 tend to zero, leaving $c_{gX} \sim 3\tilde{\alpha}^{-1}$ but $c_{gZ} \sim -\beta^{-1}$ is negative. These linear properties match with the 3D results elsewhere, and they form a stepping-stone for the ensuing nonlinear theory, although some of the nonlinear features discussed below are found in fact to yield predictions which contrast strongly with those of the linear theory.

4.2. Strong nonlinear 3D growth (regime I)

This 3D aspect again concerns high frequencies as a guideline although part of it applies also to lower frequencies (see Fig. 3). Scalings and expansions analogous to those in Sub-Section 2.2 yield the nonlinear pressure-amplitude equation

$$\left(1 + \frac{A_0}{2}\right)\frac{\partial P_{01}}{\partial t_2} - \mathrm{i}\left(\frac{\hat{A}}{\tilde{\alpha}^2}\frac{\partial^2 P_{01}}{\partial X_1^2} + \frac{\hat{B}}{\tilde{\alpha}\tilde{\beta}}\frac{\partial^2 P_{01}}{\partial X_1 \partial Z_1} + \frac{\hat{C}}{\tilde{\beta}^2}\frac{\partial^2 P_{01}}{\partial Z_1^2}\right)$$
$$= \tilde{\alpha}\left(\frac{1-\mathrm{i}}{2^{1/2}}\right)P_{01} - \frac{5\mathrm{i}}{2}\tilde{\alpha}^4 P_{01}|P_{01}|^2, \tag{4.5}$$

in the group-velocity frame corresponding to the relation $\partial P_{01}/\partial t_1 + c_{gX}\partial P_{01}/\partial X_1 + c_{gZ}\partial P_{01}/\partial Z_1 = 0$ as usual. Hence the reference frame in which the nonlinear disturbance responds is moving downstream but towards $Z = \mp\infty$ for β positive and negative respectively; the angle from the streamwise direction is c_{gZ}/c_{gX}, or $-2B_0\tilde{\alpha}/[(6 - A_0 - 2C_0)\tilde{\beta}]$. The constants appearing above are defined by

$$\hat{A} = -\{C_0 - 15 + (1 + 2A_0)\hat{F}^2 + (3A_0 + 4C_0)\hat{F}\}/2, \tag{4.6a}$$

$$\hat{B} = -\{(1 + 2A_0)2\hat{F}\hat{G} + (3A_0 + 4C_0)\hat{G} + 4B_0\hat{F}\}/2, \tag{4.6b}$$

$$\hat{C} = -\{B_0 + (1 + 2A_0)\hat{G}^2 + 4B_0\hat{G}\}/2 \tag{4.6c}$$

with $\hat{F} = \tilde{\alpha}c_{gX}$, $\hat{G} = \tilde{\beta}c_{gZ}$. As a check, for $\tilde{\beta} = 0$ (4.5) reduces to the 2D equation of Sub-Section 2.2. For the current case, removing the cross-derivative term by transforming to the co-ordinates X_1, ξ_1, where $\xi_1 = X_1 - 2\tilde{\beta}\hat{A}Z_1/(\tilde{\alpha}\tilde{\beta})$, converts (4.5) to the form

$$\left(1 + \frac{A_0}{2}\right)\frac{\partial P_{01}}{\partial t_2} - \frac{\mathrm{i}\hat{A}}{\tilde{\alpha}^2}\left(\frac{\partial^2 P_{01}}{\partial X_1^2} + \hat{H}\frac{\partial^2 P_{01}}{\partial \xi_1^2}\right) = \tilde{\alpha}\left(\frac{1-\mathrm{i}}{2^{1/2}}\right)P_{01} - \frac{5\mathrm{i}}{2}\tilde{\alpha}^4 P_{01}|P_{01}|^2 \tag{4.7}$$

with $\hat{H} \equiv (4\hat{A}\hat{C} - \hat{B}^2)/\hat{B}^2$. So the change of variables $[P_{01}, X_1, \xi_1, t_2] = [\lambda_1\hat{P}, \lambda_3\hat{X}, \lambda_4\hat{\xi}, \lambda_2\hat{T}]$, where $\lambda_1^2 \equiv 2^{1/2}/5\tilde{\alpha}^3$, $\lambda_2 \equiv 2^{1/2}(1 + A_0/2)/\tilde{\alpha}$, $\lambda_3^2 \equiv |\hat{A}2^{1/2}/\tilde{\alpha}^3|$, $\lambda_4^2 \equiv |\hat{A}\hat{H}2^{1/2}/\tilde{\alpha}^3|$, leaves us with

$$\frac{\partial \hat{P}}{\partial \hat{T}} - \mathrm{i}(\operatorname{sgn}\hat{A})\left(\frac{\partial^2 \hat{P}}{\partial \hat{X}^2} + (\operatorname{sgn}\hat{H})\frac{\partial^2 \hat{P}}{\partial \hat{\xi}^2}\right) = (1 - \mathrm{i})\hat{P} - \mathrm{i}\hat{P}|\hat{P}|^2 \tag{4.8}$$

as the governing nonlinear equation.

A particular form of solution is the plane-wave form $\hat{P} = \exp(-\mathrm{i}\hat{T} + \mathrm{i}n\hat{X} - \mathrm{i}n^2\hat{T}\,\mathrm{sgn}\,\hat{A})\,Q(\hat{\xi}, \hat{T})$, for which (4.8) reduces to

$$\frac{\partial Q}{\partial \hat{T}} - \mathrm{i}a\,\frac{\partial^2 Q}{\partial \hat{\xi}^2} = Q - \mathrm{i}Q|Q|^2 \tag{4.9}$$

where $a \equiv \mathrm{sgn}\,\hat{A}\,\mathrm{sgn}\,\hat{H}$. Hence if $a = 1$ the dispersive term leads to spatial *spreading* and the wave amplitude grows exponentially like $\exp(2\hat{T}/3)$, as in the 2D case earlier. If $a = -1$, on the other hand, the dispersive term produces spatial *focussing* and the spiky chaotic-like nonlinear behavior of Ref. 9. The solution for the value $a = -1$ is subject to fast growing short-scaled sideband instability (secondary instability) and the far-downstream response consists of multiple "spikes" growing rapidly in amplitude at a rate $\exp(2\hat{T})$ with width shrinking like $\exp(-2\hat{T})$. This nonlinear growth rate is much greater than that for the value $a = 1$ which includes the previous 2D case. In consequence the case $a = -1$ leads on downstream to the 3D higher-amplitude stage (see below) being reached more rapidly than in the 2D case.

Both of the signs $a = \pm 1$ are possible, depending on the spanwise wavenumber $\tilde{\beta}$. This can be seen from examination of certain limits as follows. First, at large $\tilde{\beta}$ we have $\hat{A} \to 3$, $\hat{B} \to -3$, $\hat{C} \to 1$, $\hat{H} \to 1/3$, and so $a = 1$, yielding the spatial-spreading response. Second, however, at small $\tilde{\beta}$ we obtain $a = -1$ hence spatial focussing. The latter case is connected in fact with the effects of slight 3D "warping" of an input 2D disturbance (Fig. 3), corresponding to reduced $|\partial_Z|$ of order $\Omega^{7/20}$, which delays all the 3D influence until the amplitude-cubed level. This *warped-wave* problem has the controlling equation, with $\sigma = \tilde{\alpha}^{-5}$,

$$(1+\sigma)\,\frac{\partial P_{01}}{\partial t_2} - \frac{\mathrm{i}}{\tilde{\alpha}^2}\left\{\left[1 + \frac{(\sigma/2-1)\sigma}{(1+\sigma)^2}\right]\frac{\partial^2 P_{01}}{\partial X_1^2} - \frac{\tilde{\alpha}\sigma}{\tilde{\beta}^2}\,\frac{\partial^2 P_{01}}{\partial Z_1^2}\right\}$$
$$= \tilde{\alpha}\left(\frac{1-\mathrm{i}}{2^{1/2}}\right)P_{01} - \frac{5\mathrm{i}}{2}\,\tilde{\alpha}^4 P_{01}|P_{01}|^2 \tag{4.10}$$

analogous to (4.7) and hence, instead of (4.9),

$$(1+\sigma)\,\frac{\partial Q}{\partial t_2} + \frac{\mathrm{i}}{\tilde{\beta}^2\tilde{\alpha}^6}\,\frac{\partial^2 Q}{\partial Z_1^2} = \tilde{\alpha}\left(\frac{1-\mathrm{i}}{2^{1/2}}\right)Q - \frac{5\mathrm{i}}{2}\,\tilde{\alpha}^4 Q|Q|^2 \tag{4.11}$$

in effect, where $P_{01} = \exp(-\mathrm{i}n^2 t_2 + \mathrm{i}nKX_1)Q$ and $K \equiv \tilde{\alpha}(1+\sigma)^{1/2}[1 + (\sigma/2-1)/\sigma(1+\sigma)^2]^{-1/2}$. Here (4.11) corresponds to the spatial-focussing value $a = -1$, implying therefore that any slight three-dimensionality in a near-planar incoming disturbance will force pronounced secondary instability to occur, followed by strong nonlinear focussing and amplitude growth.

The next stage, after the spatial focussing arises for this warped input and hence induces higher spanwise wavenumbers locally, tends to bring in the more three-dimensional effects present in (4.7)–(4.9). But by then the pressure amplitude is so large that a new, more nonlinear, balance enters play, specifically with $|P|$ increased to order $\Omega^{4/5}$ along with the scalings of Sub-Section 2.3 and $|\partial_z| \sim \Omega^{4/5}$. As a result the controlling equations

$$A_T + AA_X = -P_X\,, \tag{4.12a}$$

$$\bar{P}_{\bar{y}\bar{y}} + \bar{P}_{ZZ} = m\bar{P}_{XX} + 2\bar{P}_{XT}\,, \tag{4.12b}$$

$$\bar{P} \to P\,, \quad \bar{P}_{\bar{y}} \to A_{XX} \text{ as } \bar{y} \to 0 \tag{4.12c}$$

hold, subject to vorticity bursting from the wall layer. These are the 3D extensions of the 2D equations presented in Sub-Section 2.3, the three-dimensionality entering via the flow exterior to the boundary layer.

The two main conclusions here are the following. First, in a time of order $(9/40)\ln\Omega$ [three times faster than the pure 2D value, for instance] the slight 3D warping produces patches of higher-amplitude fully nonlinear action, as governed by (4.12). Second, this enhanced growth occurring at small $\tilde{\beta}$ for nonlinear disturbances is directly *opposite* to the implications for linear disturbances where the growth enhancement is at large $\tilde{\beta}$ (Sub-Section 4.1). Further work (see Ref. 39) indicates that this enhancement of growth by a slight warping occurs for the entire range $2^{-1/2} < \mathrm{M}_\infty \leqslant 1$ of Mach number.

4.3. Nonlinear triad interactions (regime I)

These particular triad, or three-wave, 3D interactions have a special form in the transonic regime I, due to the quasi-planar response in the boundary layer (see Fig. 4). The triads seem to be a feature specific to higher frequencies rather than to the lower frequencies where for example vortex-wave interactions tend to be triggered as described in Sub-Section 4.5 below. The governing equations here are again (2.3a–f) but with $W \equiv 0$, as stated earlier, and so the dispersion relation (2.4) holds for low-amplitude 2D or 3D waves. The nature of the dispersion relation allows many kinds of resonant triads to occur in principle, at high frequency Ω, but the particular kind which is of interest here involves a 2D wave as input upstream. In the incompressible regime (Ref. 25) triads are found to boost the otherwise slower growth rates of oblique waves and bring in 3D effects, via nonlinear interactions at the amplitude-squared level, re-distributing the energy of the faster-growing 2D wave input. In contrast, the present transonic dispersion relation identifies the oblique waves as faster growing (Sub-Section 4.1), which therefore raises the question of how the nonlinear energy re-distribution occurs here.

It can be established first that transonic triads exist as follows. The high-frequency dispersion relation is essentially (4.1b) and so three waves proportional to

$$E_1 = \exp[\mathrm{i}\{(1+s)\bar{A}X + \beta Z - (1+\mu)T\}](3\mathrm{D})\,, \tag{4.13a}$$

$$E_2 = \exp[\mathrm{i}\{\bar{A}X - T\}](2\mathrm{D})\,, \tag{4.13b}$$

$$E_3 = \exp[\mathrm{i}\{s\bar{A}X + \beta Z - \mu T\}](3\mathrm{D}) \tag{4.13c}$$

are possible in principle provided their wavenumbers and frequencies comply with (4.1b), and moreover they interact at the amplitude-squared level since

$$E_1 = E_2 E_3\,, \qquad E_2 = E_1 E_3^*\,, \qquad E_3 = E_1 E_2^*\,. \tag{4.14}$$

Here (4.1b) requires the balances

$$(1+s)^3\bar{A}^3 = (1+\mu)[2(1+\mu)(1+s)\bar{A} + \beta^2 - m(1+s)^2\bar{A}^2]^{1/2}\,, \tag{4.15a}$$

$$\bar{A}^3 = [2\bar{A} - m\bar{A}^2]^{1/2}\,, \tag{4.15b}$$

$$s^3\bar{A}^3 = \mu[2\mu s\bar{A} + \beta^2 - ms^2\bar{A}^2]^{1/2} \tag{4.15c}$$

to be satisfied. So, for given relative Mach number m, the 2D wavenumber $\bar{A}$ follows from (4.15b), leaving the equation

$$R(1+\mu) = \bar{A} + R(\mu) \tag{4.15d}$$

for the possible μ values, from (4.15a, c), where $s = R(\mu)/\bar{A}$ and $R(\mu)$ is the positive root ϕ of the polynomial equation $\phi^6 + m\mu^2\phi^2 - 2\mu^3\phi - \beta^2\mu^2 = 0$. Acceptable μ values exist for all m and β: see Fig. 4a. For example, the extreme of large β yields the asymptotes $\mu \sim \beta^{1/2}/(3\bar{A})^{3/2}$ and $s \sim 3\mu$, while in the small-β extreme we have $\mu \sim \beta^5\lambda^3$, $s \sim \beta^2\lambda\bar{A}^{-1}$ where $\lambda \equiv [2(5-2m\bar{A})]^{-1}$, provided $\beta \ll m^{-1/2}$ for large m.

It is noted here that the two oblique waves E_1, E_3 lie to the same side of the 2D one, with E_3 more oblique than E_1.

The corresponding nonlinear unsteady-flow solution now expands in the form

$$U = Y + (U_1E_1 + U_2E_2 + U_3E_3) + \text{c.c.} + O(\varepsilon^9) \tag{4.16}$$

and so on, with $\varepsilon \equiv \Omega^{-1/10}$ and U, V, P, A, Y, ∂_X, ∂_Z, $\bar{y}$ having been scaled on ε^q, $q = 5, 4, 1, 5, 5, -6, -8, -8$, in turn. Here the pressure amplitude $O(\varepsilon)$ is much less than that required for the 2D nonlinear response ($\varepsilon^{-7/2}$, Sub-Section 2.2, see also 4.2), the U-velocity disturbance amplitude is comparable with the mean flow, in (4.16), and the amplitudes U_1, P_1, etc., are slowly varying, with $\partial_T \to \partial_T + \varepsilon^q\partial_{\bar{T}}$, $\partial_X \to \partial_X + \varepsilon^q\partial_{\bar{X}}$, etc. At first order the requirements in (4.13)–(4.15) are confirmed. Then at second order the nonlinear inertial interplay brings in the connections (4.14), leading to the nonlinear triad equations

$$\left(1 + \frac{A_{0j}}{2}\right)\left[\frac{\partial P_j}{\partial \bar{T}} + c_{gX_j}\frac{\partial P_j}{\partial \bar{X}} + c_{gZ_j}\frac{\partial P_j}{\partial \bar{Z}}\right] = \bar{A}\,\frac{f_j}{h_j^{1/2}}\left(\frac{1-\mathrm{i}}{2^{1/2}}\right)P_j - \mathrm{i}\bar{A}^2h_j\bar{V}_j \tag{4.17}$$

for $j = 1, 2, 3$, where $A_{0j} = 2h_j^3/g_j^5\bar{A}^5$, $B_{0j} = \beta^2h_j^2/g_j^6\bar{A}^6$, $C_{0j} = -mh_j^2/g_j^4\bar{A}^4$, $c_{gX_j} = h_j(6 - A_{0j} - 2C_{0j})/[\bar{A}g_j(2 + A_{0j})]$, $c_{gZ_j} = -2h_jB_{0j}/[\beta(2 + A_{0j})]$ or zero, $f_j = g_j/h_j$ where $g_j = (1 + s, 1, s)$, $h_j = (1 + \mu\ 1, \mu)$, and $\bar{V}_j = (f_2f_3P_2P_3,\ f_1f_3P_1P_3^*,\ f_1f_2P_1P_2^*)$ defines the nonlinear interaction terms in (4.17).

The governing equations (4.17) are analogous to those in Ref. 25 and the coefficients are such that no finite-time or -distance breakdown is to be expected. Instead the nonlinear amplitudes are likely to increase exponentially downstream. Computations (e.g. as for (4.18a–c) below, in Fig. 4b) should be of interest both here and for the three-oblique-wave interactions possible. In addition, interactions can also occur, at the same amplitude sizes, for two extra oblique modes present on the other side of the 2D one, pointing to a pair of triads inter-linked by the common 2D wave.

Once again the extremes of small and large β allow some simplification. If β is large there are two almost identical, relatively fast growing, oblique waves P_1 and P_3. If we scale $[P_1, P_2, P_3, T]$ as $[1, \beta^{-1/4}, 1, \beta^{-1/4}]$, i.e. relatively small amplitudes, we retain the nonlinear terms but lose the small growth term in the 2D wave. Factoring out $O(1)$ constants we are then left with

$$P_{1T} = \frac{(1-\mathrm{i})}{\sqrt{2}}\,P_1 - \mathrm{i}P_2P_3\,, \tag{4.18a}$$

$$P_{2T} = -\mathrm{i}P_1P_3^*\,, \tag{4.18b}$$

$$P_{3T} = \frac{(1-\mathrm{i})}{\sqrt{2}} P_3 - \mathrm{i}P_2^* P_1 \,. \tag{4.18c}$$

See computations in Fig. 4b. If β is small there are two almost identical but nearly 2D waves P_1, P_2 with slow growth and one almost stationary but very oblique 3D wave, P_3. It is P_3 that is responsible for extracting energy from the mean flow. Scaling $[P_1, P_2, P_3, T]$ as $[\beta^{-3/2}, \beta^{-3/2}, \beta^{5/2}, \beta^{1/2}]$ and again factoring out $O(1)$ constants yields the equations

$$P_{1T} = -\mathrm{i}P_2 P_3 \,, \tag{4.19a}$$

$$P_{2T} = -\mathrm{i}P_1 P_3^* \,, \tag{4.19b}$$

$$P_{3T} = \frac{(1-\mathrm{i})}{\sqrt{2}} P_3 - \mathrm{i}P_1 P_2^* \,. \tag{4.19c}$$

These reduced sets need to be treated numerically to follow the triads' behavior. In both cases there is the possibility of nonlinear interaction activating the 2D modes and possibly causing an increased growth on the more rapid time-scales associated with the oblique waves.

4.4. Three-dimensional effects in transonic regime II

Many of the 3D effects present in the alternate transonic regime II are described already in Section 3. The main additional remark to make here is that, since the non-separated flow is always stable to small disturbances in this regime, most of the nonlinear 3D interactions just investigated (Sub-sections 4.2, 4.3) cannot arise here since they are relatively low-amplitude phenomena. A possible exception is the higher-amplitude stage corresponding to (4.12). Apart from that, transition in this regime seems likely to be triggered either by (2D or 3D) separation as in 3.3 or by the nonlinear 3D interactions discussed in the next sub-section, both of these being in a sense *by-pass* transition processes.

4.5. Distinct 3D regimes and interactions

There are two extra nonlinear interactions to consider briefly, both of which are distinctly 3D in nature and rather divorced from the previous transonic regimes.

One is identified essentially in Ref. 21, as a so-called major limit. Its governing equations are (2.3) in effect but with the spanwise pressure gradient P_Z added to (2.3c) and with the contributions $\bar{P}_{XX}$, $\bar{P}_{XT}$ omitted in the TSP balance, i.e.

$$\bar{P}_{\bar{y}\bar{y}} + \bar{P}_{ZZ} = 0 \,, \tag{4.20a}$$

yielding a P–A relation in terms of a Cauchy integral in Z. This transonic 3D interaction is intriguing partly because it is independent of the Mach number, applying therefore to both regimes I, II in particular, and partly because it is very unstable on linear grounds (hence the term 'major', Ref. 21), more so than the other interactions found. It also exhibits strong nonlinear growth for sufficiently oblique 3D waves, due to the high-frequency dispersion relation

$$\alpha(\alpha^2 + \beta^2) = \beta\Omega \tag{4.20b}$$

which shows that the streamwise and spanwise group velocities are minimum and maximum, respectively, for waves at a critical angle

$$\theta\text{–crit} = \sin^{-1}(3^{1/4}/2^{1/2}) = 68.53^{\circ} \tag{4.20c}$$

from the streamwise direction, corresponding to $\alpha^2 = 3^{1/4}(3^{1/2} - 1)/2^{3/2}$. Consequently an amplitude-cubed nonlinear balance, analogous to those in Sub-Sections 2.2, 4.2, leads after some working to the equivalent of (4.9), with the angle (4.20c) corresponding to the crossover from the value $a = 1$ to $a = -1$. The strong nonlinear 3D growth, associated with spatial focussing, occurs for wave angles exceeding the critical value (4.20c).

This enhanced 3D growth, at the *larger* wave angles, contrasts with the finding in (4.2) of enhanced 3D growth at *small* wave angles.

The other remaining aspect concerns vortex-wave interactions, which can occur in all the 3D transonic regimes. The typical controlling equations consist of (2.3a–c) for the vortex over a long spatial scale, with P_X absent, coupled with an ordinary-differential equation for the wave-pressure acting on a shorter scale; the nonlinear coupling here is through the vortex wall-shear, which affects the coefficients in the wave-pressure equation, and through an amplitude-squared forcing exerted by the wave pressure on the vortex motion. The details are given in Ref. 28 for interactions between vortex flow and compressible TS waves, while Ref. 27 addresses the interactions arising with compressible Rayleigh waves. Even though the wave amplitude is relatively small it affects the mean flow at leading order, i.e. completely alters the mean-flow profiles, and so the vortex-wave interactions are potentially powerful phenomena. Moreover, they can arise at any Mach numbers including those addressed in Sections 2, 3, although the flow structures involved are not necessarily the same as in those sections. Vortex-wave interaction can also provide a by-pass transition mechanism since it does not rely on the prior existence of linear instabilities; the full properties of these interactions are still under investigation.

5. Further discussion

The main result of this work on transonic transition is that the mechanisms behind the three major factors described at the outset, (a) substantial external-flow deceleration, (b) rapid boundary-layer thickening, (c) 3D nonlinear interactions, have been identified.

Concerning factors (a), (b), two predominant types of unsteady 2D transonic interaction have been found, in Sections 2, 3. The first which acts as a springboard for the rest of the theory is governed by the linearized-TSP equations linked with the unsteady IBL equations via pressure-displacement interaction, as studied in Section 2. This type captures gradual transition and is found to have some significant properties, but it cannot account readily for the considerable external deceleration, e.g. with a shock, which seems crucial according to (a) above. In addition, many of its transition implications examined turn out to be simply quasi-incompressible, which, although of interest, appears to restrict its relevance here. The second type of interaction, by comparison, seems most relevant to (a) and (b). Its governing equations are the nonlinear TSP equations and the quasi-steady IBL equations, linked together through pressure-displacement interaction as discussed in Section 3. This is a relatively low-frequency response and can incorporate, as required, the effects of an unsteady external shock or other substantial external behavior, while allowing for transition and/or separation downstream in the boundary layer. Another advantage here is that the

linkage captured in Section 3, if self-sustaining as seems likely, provides the means for by-pass rather than gradual transition, which again is as required at the outset. The powerful by-pass arises here for two reasons: on the one hand, nonlinear instability is very sensitive to the boundary layer's pressure-displacement response, with the factor (b) above being found to de-stabilize the flow readily [see Sub-Section 3.3]; and, on the other, the shock-flutter phenomenon can be regarded as one of receptivity, i.e. given a shock oscillation, say due to free-stream unsteadiness, Sub-Section 3.3 enables the boundary-layer effects to be determined and then an estimate to be made for the resonance criterion between the shock oscillation and the internal instability.

The factor (c) concerning 3D transition effects is likewise a very sensitive one in the transonic range. The 3D effects tend to matter most in the motion just outside the boundary layer, due essentially to the reduction in the typical streamwise length scales, induced by transonic flow. This therefore produces certain novel 3D interactions, as addressed in Section 4. Most of these 3D responses can start from secondary instability of a 2D input upstream but their subsequent nonlinear behavior is of most interest, as it often contrasts with the linear predictions. In particular, new nonlinear resonances can occur (Sub-Section 4.3) between a 2D input disturbance and two 3D oblique disturbances, throughout the transonic range, and increase the overall growth rate. Again, nonlinear 3D disturbances alone can focus, and amplify strongly, if they are directed sufficiently far outside or well inside the wave-Mach-cone direction (see Sub-Sections 4.2, 4.5). An even slight 3D warping in a near-planar input disturbance (Sub-Section 4.2) causes a similar focussing and strong amplification downstream. Thus in 3D there appear to be nonlinear mechanisms which can pour energy into the less oblique disturbances, for instance, and force them to acquire full nonlinear status downstream, i.e. produce transition, much sooner than would be the case in 2D. It is clear overall that these 3D effects, and vortex-wave forms like that in Sub-Section 4.5, are very powerful and "dangerous" in the transonic regime of concern.

Several issues which are not so directly relevant, as yet anyway, should also be mentioned for the record. One is the alternative scenario suggested by analogy with Refs 17, 18. If the strength or upstream movement of the shock is sufficiently large and separation occurs, then the local reversed-flow breakdown of Ref. 18 can arise (within the quasi-steady IBL of the regime in Section 3), thereby bringing about a collapse of the otherwise large-scale separation for instance, at a finite time. The collapse, accompanied by fast transition, tends to reduce the downstream pressure however and hence decreases the shock strength. This in turn reduces the flow reversal and so suppresses the local breakdown and transition. So the downstream pressure can then rise again and the pattern may repeat itself, giving overall a self-sustaining oscillation between the shock and the separation. A very similar pattern can be envisaged for the unsteady IBL in the regime of Section 2, due to the unsteady finite-time break-up of Ref. 17 for such IBL flows. Obviously, 2D and 3D computations based on the formulations of Sections 2–4 would be helpful here, and indeed this aspect of transition, which is relevant to intermittency, is still the subject of separate continuing research even in the incompressible regime. The second issue, given the sensitivity of the transonic transition to boundary-layer thickening (see (b) above), surrounds the various kinds of separation possible, principally whether the separation is small- or large-scale. One kind is examined in Section 3. Another kind however is for the transonic regime of Section 2 where in effect unsteadiness acts explicitly within the boundary layer, adding contributions $\partial U/\partial T, \partial S/\partial T$, $\partial(S+A)/\partial T$ to (3.8a–c) respectively, which then alters the responses (3.9a, c), (3.10). For instance, the TSP coupling leads here to the dispersion relation $\alpha^3 S_0 - \alpha^2\Omega \pm \Omega^2(2\Omega/\alpha - m)^{1/2} = 0$, or $\alpha = \pm c^2(2c-m)^{1/2}/(c-S_0)$, in the case where $-A_0 \equiv S_0$. This again

admits neutral subsonic or supersonic waves, as in Section 3, and some supersonic long-wave growth, but the violent instability of the Kelvin–Helmholtz type that occurs for the pure subsonic or supersonic boundary layer (Ref. 23) is suppressed in the current transonic range. Third, other aspects of the theory are summarized in the Appendices. Finally here, the influences of surface cooling are considered in recent joint work involving the authors, Ref. 24. There it is shown that the cooling not only accentuates inviscid instability, in line with previous predictions, but also greatly enhances the viscous-inviscid TS growth, eventually making it even exceed that of the inviscid modes. This again is a dangerous feature.

The main implications in the nacelle-flow context with which we began appear to be the following. While more research is undoubtedly needed on the mechanisms found for (a)–(c) above, the results so far tend to indicate that suppression of the features, or dangers, (a)–(c) is desirable if transition and its consequent flow penalties are to be avoided in practice. Thus the 3D geometrical warping mentioned at the start is undesirable as it can lead to danger (c). Pronounced adverse pressure gradients are equally undesirable, as they can provoke the linkage between the dangers (a), (b); and smooth surfaces seem necessary, to avoid by-pass transition throughout the transonic range.

The further research just mentioned is to be based on the present theoretical treatment of the Navier–Stokes equations which leads to reduced systems of nonlinear unsteady equations capturing the appropriate external-internal interaction, at the high Reynolds numbers of practical interest. Previous such studies have established a firm tie-in with boundary-layer transition experiments in the incompressible case, while the present study lays the foundations for the transonic-flow features (a)–(c) in particular, for the approximate range 0.8–1.2 in local Mach number. The nonlinear effects discussed here are believed to be very strong candidates for explaining the transonic nacelle transition process, and further analytical and computational work based on the mechanisms found above for (a)–(c) is under way. Comments on the alternative e^N method (see e.g. Refs 13–16) should also be made here. In brief, the quasi-parallel e^N methodology which is based on linear Orr–Sommerfeld theory seems without doubt of high engineering value for gradual or natural transitions which start from initially linear disturbances, in a mildly-varying and low-disturbance environment. It is likely to be of much less value and reliability in the stronger, e.g. by-pass, transition processes like that operating in the transonic nacelle flow (see above), however, simply because of the nonlinear nature of such transitions. By-pass transition by definition requires a nonlinear theory to be applied. The current aim is to develop the relevant nonlinear theory (e.g. [17, 31, 40, 41]). Along with this, subsequent comparisons can be made between the theory and the earlier methodology for weaker environments, both as a check and as an alternative method, and then the enhancement of transition as nonlinearity increases can be tracked.

Our conclusion, then, is that the transition in certain transonic flows, including the nacelle flow, is a strong nonlinear phenomenon, produced by the linkage between the boundary layer and the external unsteady transonic flow, as in the mechanisms found for the major features (a)–(c). Other transonic-flow configurations may be described by lower-amplitude transition. The broad area seems to merit much further research, and it is hoped that clarification of the transition criteria describing the dependence of transonic transition on the disturbance environment and pressure gradients will emerge from the research. Extensions, to transonic flow, of the nonlinear transition predictions in Refs 17, 40, 41, 43 in particular could prove of much interest.

Much of this work was done during 1988–89 and appeared originally as Ref. 42 in 1989,

while further details on the 3D theory, on upstream influence, on the resonant triads described in Section 4 (including their solution at large times), and on the large-m limit, are given in Ref. 39. The authors wish to thank Drs Wes Lord, Jim Carter, Mike Werle and colleagues for numerous very helpful suggestions and comments, and United Technologies, AFOSR (grant no. 89-0475) and S.E.R.C., U.K., for financial support.

Appendix A – The connections with other flow regimes

Here the links between the theory and results in the main text and those for certain other flow regimes are described.

First, the 3D version of the transonic interaction I addressed in Section 4 matches at large $|\bar{m}|$ with the theory of [21, 22] in the supersonic or subsonic case. The other 3D interaction in Section 4, for waves directed well outside the wave-Mach cone, yielding larger linear growth rates, is identical with one in [21]. In the former case the spanwise pressure gradient is negligible inside the boundary layer and the outer flow is significantly unsteady, whereas in the latter case the streamwise pressure gradient is negligible in the (quasi-steady) outer flow, producing a corresponding lack of Mach-number dependence.

Second, the 2D wave-packet result in Section 2.2 connects with that for incompressible or subsonic flow in [20] when $m \to -\infty$ in (2.10a), with $\alpha, \partial_{t_2}, P_{01}$ being of order $|m|^{3/8}$, $|m|^{1/4}, |m|^{-3/8}$ in turn, as $|m|$ becomes of order $\mathrm{Re}^{1/9}$. The nonparallel-flow result (2.15) matches similarly.

A third link is between the high-frequency dispersion relation (2.5) and that for inviscid inflexional waves where the compressible Rayleigh equations holds (Ref. 31). This link is analogous to that for the nonlinear theory as discussed in Sections 2.3, 2.4, and it occurs for $\partial_X, \partial_T, \mathrm{M}_\infty^2 - 1$ and the wavespeed c becoming of size $\mathrm{Re}^{1/2}\varepsilon^{3/2}\alpha_0$, $\mathrm{Re}^{1/2}\varepsilon^{5/2}\Omega_0$, $\varepsilon\bar{m}$ and $\varepsilon\Omega_0/\alpha_0 = \varepsilon c_0$ respectively, for small ε. These scales match with those obtained from analyzing the compressible Rayleigh equation directly. Higher-order matching however, which controls the small growth rates, seems to bring in critical-layer effects in an intermediate viscous-inviscid regime (cf. Ref. 21), the scales involved then depending on the wall conditions. Thus for an *adiabatic* wall we have $c \sim \delta$, the length scale $L \sim \delta^7$, the time scale $T \sim \delta^6$, with $\mathrm{M}_\infty^2 - 1 \sim \delta$, a lower region (including the critical layer) of thickness $\mathrm{Re}^{-1/2}\delta$, a Stokes-layer thickness $\mathrm{Re}^{-1/2}\delta^3$ and an outermost (unsteady) region of thickness $\mathrm{Re}^{1/2}\delta^{21}$, where $\delta \sim \mathrm{Re}^{-1/17}$. For a *cooled or heated wall*, in contrast, $c \sim \delta$, $L \sim \delta^5$, $T \sim \delta^4$, $\mathrm{M}_\infty^2 - 1 \sim \delta$ and the thickness above become in turn $\delta\,\mathrm{Re}^{-1/2}$, $\mathrm{Re}^{-1/2}\delta^2$, $\mathrm{Re}^{1/2}\delta^{18}$, with now $\delta \sim \mathrm{Re}^{-1/13}$. In each case v expands in the form $\mathrm{Re}^{-1/3}L^{-1}\delta(v_0 + \delta v_1 + \delta^2 v_2 + \cdots)$, say, and the critical layer is required to smooth out the logarithmic irregularity, in v_2, for the adiabatic wall, or in v_1 for the cooled/heated wall, which then provokes a phase shift of $-\pi$ for linear disturbances. This shift balances the phase shift produced by the Stokes layer. Nonlinear effects can come into play at low amplitudes inside the critical layer.

Finally, the progression from lower-branch through upper-branch to compressible-Rayleigh properties, at increasing m, ties in with the cut-off enforced by the required decay of disturbances in the free stream. The disturbances must be subsonic relative to the free stream (Refs 21, 35), i.e. $c > 1 - \mathrm{M}_\infty^{-1}$ or, in our notation $c > \bar{m}/2$, where the speed $1 - \mathrm{M}_\infty^{-1}$ is that of the slowest characteristic or sound wave in the free stream. Increasing $\bar{m}$ therefore forces c to increase, producing a move away from viscosity-induced TS waves.

Appendix B – Supercritical modes

Here the effect of the weakened viscous-inviscid interaction as $\bar{m} \to \infty$ on the waves mentioned at the end of Appendix A is considered for 2D motions.

As $\bar{m} \to \infty$ the scales are

$$[U, V, P, A] \sim [\bar{m}, \bar{m}^{-1}, \bar{m}, \bar{m}],$$

$$[\partial_X, \partial_T, \partial_Y, \partial_{\bar{y}}] \sim [\bar{m}^{-3}, \bar{m}^{-2}, \bar{m}^{-1}, \bar{m}^{-7}]$$

and (2.3e) becomes

$$\frac{1}{\bar{m}^9} \bar{P}_{\bar{y}\bar{y}} = \bar{P}_{XX} + 2\bar{P}_{XT} \tag{B1}$$

whilst the lower-deck equations (2.3a, b), though in new variables, are unchanged. Here (B1) shows that as $\bar{m}$ increases the determination of the wave speed becomes inviscid to first order and governed by the right-hand side of (B1). Essentially any disturbance moves downstream with the speed of the slowest sound wave in the freestream. Moving in this travelling frame, in which the unsteadiness is slow, $O(\bar{m}^{-9})$, i.e. making the transformation

$$\partial_T \to -\frac{1}{2}\partial_X + \bar{m}^{-9}\partial_{\hat{T}}, \tag{B2}$$

alters (2.3) to

$$\begin{aligned} &\bar{P}_{\bar{y}\bar{y}} = 2\bar{P}_{X\hat{T}}, \\ &-\frac{1}{2} U_X + UU_X + VU_Y + \frac{1}{\bar{m}^9} U_{\hat{T}} = -P_X + U_{YY}, \\ &\bar{P}_{\bar{y}} = A_{XX}, \quad P = \bar{P}, \text{ at } \bar{y} = 0 \quad \text{and} \quad U \sim Y + A \text{ as } Y \to \infty. \end{aligned} \tag{B3}$$

This nonlinear system with $\bar{m} = \infty$ has a lower-deck equation corresponding to a boundary layer over an upstream-moving wall and is subject to possible singularities. A linearised version for, say, a small-amplitude wave of frequency Ω yields the dispersion relation

$$\frac{1}{(\mathrm{i}\alpha)^{1/3}} \frac{(2\omega\alpha)^{1/2}}{\alpha^2} \frac{Ai'(\xi_0)}{k} = 1 \tag{B4}$$

with $\xi_0 = -(\mathrm{i}\alpha)^{1/3}/2$ and $\mathrm{i}\alpha = \partial_X$ fixed by (B2) to be $2\mathrm{i}\Omega$. Thus (B4) determines $-\mathrm{i}\omega = \partial_{\hat{T}}$.

The $\bar{m}^{-9}$ term in (B3) affects matters at a higher order. We may gauge its effect on a slow spatial growth-nonlinearity balance for an $O(1)$ value of ω and derive a Stuart–Watson equation for a wave near the neutral point, determined from (B4) via a suitable multi-scale analysis of the following system,

$$\begin{aligned} &\bar{P}_{\bar{y}\bar{y}} = 2\bar{P}_{X\hat{T}}, \\ &\varepsilon^n U_{\hat{T}} - \frac{1}{2} U_X + (\lambda Y + \varepsilon U)U_X + (\lambda + \varepsilon U_Y)V = -P_X + U_{YY}, \\ &U_X + V_Y = 0, \\ &U \to A \text{ as } Y \to \infty, \quad \text{and} \quad \bar{P}_{\bar{y}} = A_{XX}, \quad \bar{P} = P, \text{ at } y = 0 \end{aligned} \tag{B.5}$$

with the small parameter $\varepsilon = (\bar{m}^{-9}, \bar{m}^{-9/2}, \bar{m}^{-3})$, $P \sim (\bar{m}^{-7}, \bar{m}^{-3/2}, 1)$ for $n = 1, 2, 3$. Here $\lambda(x)$ is the slowly varying skin-friction parameter. For $n \geqslant 3$ the disturbance amplitude is so great and the development is so rapid that the weak $\partial_{\bar{T}}$ feedback into the boundary layer has no influence. This is similar to the behavior in Appendix C, where a weakly nonlinear analysis for large ω is presented.

If $\bar{m}$ becomes of the order of a power of Re, the expansion behind (2.3) fails due to the travelling frame moving, in the time associated with $\partial_{\bar{T}}$ and the decay of disturbances in the free stream, a distance sufficiently large that the weaker effects of compressibility or boundary-layer non-parallelism become important. The effects of a cooled/heated wall, adiabatic wall or non-parallelism balance the $\partial_{\bar{T}}$ unsteadiness in the boundary layer when $M_\infty^2 - 1 \sim Re^{-1/10}$, $Re^{-1/11}$, $Re^{-1/12}$ respectively. These are higher-order effects for the disturbance primarily governed by (B3) with $\bar{m} = \infty$, although a multi-scale type of analysis of the Navier–Stokes equations could gauge their effects. However when $M_\infty^2 - 1 \sim Re^{-1/12}$ the triple-deck structure moves an $O(1)$ distance downstream, the normalization (2.1a–c) implicit in (B3) varies with T, and the non-parallelism becomes nontrivial.

On increasing $M_\infty^2 - 1$ to $O(1)$ the triple-deck structure moves an $O(\mathrm{Re})$ distance downstream over the time scale of the interaction. What this represents is as yet unclear. The weakening interaction implied in a stationary triple-deck structure suggests that any disturbances on a flat plate must decay normally within the boundary layer itself, or be governed by the supersonic version of the viscous interaction which allows radiating waves but yields only stable (linear) waves. Again, the linear stability of the boundary layer is more likely to be determined by the properties of oblique viscous-inviscid waves, lying outside of the wave cone (Ref. 21), which widens as $\bar{m}$ increases, than by the 2D structures mentioned here whose form is necessitated by the requirement of decay of disturbances in the free stream.

Appendix C – Further aspects of the transonic regime I

Values of the relative Mach number $\bar{m}$ different from those in Section 2 can give rise to new linear and nonlinear balances, some of which are considered below. The first concerns $\bar{m}$ of order $\Omega^{1/2}$ at high frequencies, for which (2.5) suggests that $\alpha \sim 2m^{-1} + O(m^{-6})$ in the supercritical case. The relative error in this result, combined with the weak effects of viscous growth, dispersion and nonlinearity indicated by (2.10a), point to the scales

$$m = m_1 \Omega^{1/2}, (X, Y, T, \bar{y}) \rightarrow O(\Omega^{-1/2}, \Omega^{-1/2}, \Omega^{-1}, \Omega^{1/2}), \tag{C1}$$

$$(U, V, P, A) \rightarrow O(1, 1, \Omega^{1/2}, 1), \tag{C2}$$

followed by the multi-scaling

$$\partial_T \rightarrow -\frac{m_1}{2}\partial_X + \Omega^{-1/2}\partial_t, \qquad \partial_t \rightarrow [\partial_{t_0} + \Omega^{-1/2}\partial_{t_1} + \Omega^{-1}\partial_{t_2} + \cdots], \tag{C3}$$

$$\partial_X \rightarrow \partial_{X_0} + \Omega^{-1/2}\partial_{X_1} + \Omega^{-1}\partial_{X_2} + \cdots \tag{C4}$$

for the governing equations, which now have the form

$$-\frac{m_1}{2} U_X + \Omega^{-1/2}(U_t + UU_X + VU_Y) = -P_X + U_{YY}, \tag{C5}$$

$$\bar{P}_{\bar{y}\bar{y}} = 2\bar{P}_{Xt}\,, \tag{C6}$$

replacing (2.3b, e) respectively, in view of the downstream travel at the sound speed in (C3). The nonlinear theory for a wave proportional to $\exp(\mathrm{i}\alpha X_0 - \mathrm{i}\omega t_0)$ in this moving frame at leading order proceed much as in Section 2.2 but with some differences. Thus first-order terms yield the dispersion relation

$$m_1(2\omega\alpha)^{1/2} = 2\alpha^2\,; \tag{C7}$$

second-order terms produce harmonics, a mean-flow correction, and the modified-group-velocity result

$$\frac{\partial P_{01}}{\partial t_1} + c_g \frac{\partial P_{01}}{\partial X_1} = \frac{\mathrm{i}\alpha^{10}}{2b^5} P_{01} \tag{C8}$$

where $c_g = 3\omega\alpha^{-1}$, $b = \alpha m_1/2$; and at third order the pressure-amplitude equation

$$\begin{aligned} &\frac{b}{\alpha^5}\frac{\partial P_{01}}{\partial t_2} - \frac{3\mathrm{i}}{2\alpha^2 b}\frac{\partial^2 P_{01}}{\partial X_1^2} - \frac{5\alpha^4}{2b^4}\frac{\partial P_{01}}{\partial X_1} \\ &\quad = \frac{\alpha(1-\mathrm{i})}{2^{1/2}b^{5/2}} P_{01} - \frac{7\mathrm{i}\alpha^{10}}{8b^7} P_{01} - \frac{5\mathrm{i}\alpha^4}{2b^4} P_{01}|P_{01}|^2 \end{aligned} \tag{C9}$$

is obtained. Since the constant b must equal one, however, a moving-frame transformation applied to (C9) shows that in the end there is no qualitative difference from the nonlinear balance (2.10a) and its results summarized in Section 2.2.

The second new stage that we have studied is at still larger $|\bar{m}|$, where the interaction between the inner and outer flows weakens, e.g. $|\bar{m}| \sim \Omega^{5/8}$ or $\Omega^{11/14}$. Omitting the details, we find again that, despite certain new balances appearing, in a frame moving essentially with the sound speed the amplitude equation for weak nonlinearity exhibits no significant differences from (2.10a).

Third, in contrast, is the fully nonlinear stage at high frequencies where the boundary layer is governed by

$$-\frac{m_1}{2} A_X + AA_X = -P_X \tag{C10}$$

instead of (2.3a–d), and the TSP equation (2.3e) is replaced by

$$\bar{P}_{\bar{y}\bar{y}} = 2\bar{P}_{XT}\,. \tag{C11}$$

This stage results for example from increased amplitudes in the stages mentioned just above. Here (C10), (C11) with the appropriate boundary conditions lead to a single nonlinear integral equation [related to (2.12a, b) in a moving frame although the boundary layer is quasi-steady here]

$$(B-1)^2 = 1 - \int_0^T \int_{-\infty}^X \frac{\partial^2 B(\xi,\eta)/\partial\xi^2 \,\mathrm{d}\xi\,\mathrm{d}\eta}{(T-\eta)^{1/2}(X-\xi)^{1/2}} \tag{C12}$$

for $B(X, T) \equiv 2m_1^{-1}A$, with normalized X, T coordinates, subject to $B \to 0$ as $|X| \to \infty$. It is

noted that the cases $B = -1, 0$ correspond to stationary motion and sonic travel respectively in the laboratory frame. Viscous sublayer properties can still be substantial, as described in Sub-Section 2.3, but the properties of the inviscid equation (C12) alone, and its 3D counterpart, may well be of much interest. This is reinforced to some extent by the finding in Ref. 17 that break-up of the full system (2.1) is controlled by predominantly inviscid features. A computational investigation of (C12) would seem well worthwhile.

References

1. T.J. Bogar, Structure of self-excited oscillations in transonic diffuser flows. *AIAA Journal* 24 (1986) 54–61.
2. D.S. Dolling and L. Brusniak, Separation shock motion in fin, cylinder and compression ramp-induced turbulent interactions. AIAA Paper 87–1368 (1987).
3. D.S. Dolling, Review of separation shock-wave dynamics in supersonic interactive flows. *Proc. Roy. Aero. Soc. Mtg., Prediction and Exploitation of Separated Flows.* April 1989, London (1989).
4. E.R. Van Driest and C.B. Blumer, Boundary-layer transition: freestream turbulence and pressure-gradient effects. *AIAA Journal* 1 (1963) 303.
5. J. Dunham, *Predictions of Boundary-Layer Transition on Turbomachinery Blades.*
6. D. Arnal, Description and prediction of transition in two-dimensional compressible flow. AGARD Report, 709 (2-1 to 71) (1984).
7. M.V. Morkovin, Recent insights into instability and transition to turbulence in open-flow systems. AGARD-AG-236, and 1988, AIAA Paper No. 88-3675.
8. F.T. Smith, Interactions in boundary-layer transition. Invited Lecture, I.C.T.A.M. Conf., Aug. 1988, published by Springer-Verlag (1989).
9. W.B. Roberts, Calculation of laminar separation bubbles and their effect on airfoil performance. AIAA paper no. 79-0285, New Orleans (Jan. 1979).
10. B.J. Abu-Ghannam and R. Shaw, Natural transition of the boundary-layer-the effects of turbulence, pressure gradient, and flow history. *J. Mech. Eng. Sci.* 22 (1980) 213–228.
11. R. Narashimha, The laminar-turbulent transition zone in the boundary layer. *Progr. Aerospace Sci.* 22 (1985) 29–80.
12. J.P. Gostelow and A.R. Blunden, Investigations of boundary layer transition in an adverse pressure gradient. Trans. ASME 88-GT-298, June 1988, Amsterdam (1988).
13. A.M.O. Smith and L.N. Gamberoni, Transition, pressure gradient and stability. *Theory, Proc. 9th Int. Congr. on Applied Mechs.*, Brussels. 56 (1956) 234–244.
14. J.L. Van Ingen, A suggested semi-empirical method for the calculation of the boundary-layer region, V.T.H., Delft, Netherlands, Rept. VTH71 (1956).
15. T. Cebeci and D.A. Egan, The effects of wave-like roughness on transition. AIAA paper 88-0139 (1988).
16. T. Cebeci, Numerical instabilities in the calculation of laminar separation bubbles and their implications. *AIAA Journal.* (Tech. Note) 27 (1989) 656–666.
17. F.T. Smith, Finite-time break-up can occur in any unsteady interacting boundary layer. *Mathematika* 35 (1988) 256–273.
18. F.T. Smith, A reversed flow singularity in interacting boundary layers. UTRC Report 88-12 (and *Proc. Roy. Soc.* A420 (1988) 21–52).
19. F.T. Smith, The strong nonlinear growth of 3D disturbances in boundary-layers [extended and submitted to Mathematika, 1992, with R.G.A. Bowles and P.A. Stewart]. UTRC Report 86-10 (1986).
20. F.T. Smith, Two-dimensional travel, growth and spreading in boundary layers. UTRC Report 85-36 (and *J. Fluid Mech.* 169 (1986) 353–377) 1985.
21. F.T. Smith, On the first mode instability in subsonic, supersonic or hypersonic boundary layers. UTRC Report 87-52 (and *J. Fluid Mech.*, 198 (1989) 127–153) 1987.
22. F.T. Smith and O.R. Burgraff, On the development of large-sized, short-scaled disturbances in boundary layers. *Proc. Roy. Soc.* A399 (1985) 25–55.
23. S.N. Brown, H.K. Cheng and F.T. Smith, Nonlinear instability and breakup of separated flow. *J. Fluid Mech.* 193 (1988) 191–216 (and Smith, UTRC Report 85-55).
24. S. Seddougui, R.I. Bowles and F.T. Smith, Surface-colling effects on compressible boundary-layer instability, and on upstream influence. *European J. Mechs.* B10 (1991) 117–145.
25. F.T. Smith and P.A. Stewart, The resonant-triad nonlinear interaction in boundary layer transition. UTRC Report 86-26 (and *J. Fluid Mech.* 179 (1987) 227–252) 1986.
26. P.A. Stewart and F.T. Smith, Three dimensional instabilities in steady and unsteady non-parallel boundary

layers, including effects of Tollmien–Schlichting disturbances and cross flow. *Proc. Roy. Soc. Lond.* A409 (1987) 229–248.
27. P. Hall and F.T. Smith, The nonlinear interaction of Tollmien–Schlichting waves and Taylor Gortler vortices in curved channel flows. flows. *Proc. Roy. Soc.* A417 (1988) 255–282 and *Euro J. Mech.* B8 (1989) 179–205.
28. F.T. Smith and A.G. Walton, Nonlinear interaction of near planar Tollmien–Schlichting waves and longitudinal vortices in boundary layer transition. *Mathematika* 36 (based on ICASE Report 86-66) (1989).
29. R.I. Bowles, Application of nonlinear viscous-inviscid interactions in liquid layer flows and transonic boundary layers transition. Ph.D. Thesis, Univ. of London (1990).
30. P. Hall and F.T. Smith, On strongly nonlinear vortex-wave interactions in boundary layer transition. *J. Fluid Mech.* 227 (1991) 641–666.
31. S.N. Brown, A.F. Khorrami, A. Neish and F.T. Smith, In hypersonic boundary-layer interactions and transition. *Trans. Roy. Soc.* A 335 (1991) 139–152.
32. F.T. Smith, D. Papageorgiou and J.W. Elliott, An alternative approach to linear and nonlinear stability calculations at finite Reynolds numbers. *J. Fluid Mech.* 146 (1984) 313–330.
33. O.S. Ryzhov, private communication (1991).
34. R.V. Brotherton-Ratcliffe and F.T. Smith, Complete breakdown of an unsteady interacting boundary layer (over a surface distortion or in a liquid layer). *Mathematika* 34 (1987) 86–100.
35. L.M. Mack, Boundary layer stability theory. AGARD Report, 709 (3-1 to 8-1) (1984).
36. L.M. Mack, Linear stability theory and the problem of supersonic boundary-layer stability. *AIAA Journal* 13 (1975) 278–289.
37. H.M. Brilliant and T.C. Adamson, Shockwave-boundary layer interactions in laminar transonic flow. *AIAA Journal* 12 (1974).
38. R.J. Bodonyi and F.T. Smith, Shock-wave laminar boundary layer interaction in supercritical transonic flow. *Computer and Fluids* 14 (1986) 97–108.
39. R.I. Bowles, Linear and nonlinear disturbances in transonic boundary layers. U.T.R.C. Report, 91–33 (1991).
40. V.J. Peridier, F.T. Smith and J.D.A. Walker, Vortex-induced boundary-layer separation, Parts 1 and 2. *J. Fluid Mech.* 232 (1991) 99–131 and 133–165.
41. J.M. Hoyle, F.T. Smith and J.D.A. Walker, On sublayer eruption and vortex formation. *Comp. Phys. Commns.* 65 (1991) 151–157.
42. R.I. Bowles and F.T. Smith, On boundary-layer transition in transonic flow. U.T.R.C. Report 89-26 (1989).
43. F.T. Smith and R.I. Bowles, Transition theory and experimental comparisons on (I) amplification into streets and (II) a strongly nonlinear break-up criterion. *Proc. Roy. Soc.* A 439 (1992) 163–175.